UNIVERSIDADE D COIMBRA
FACULDADE DE CIÊNCIAS E TECNOLOGIA

DIOGO ANTÓNIO BORGES DE JESUS

Accelerometer signals for detection of pulse presence and blood pressure inference

Thesis submitted to the
University of Coimbra for the degree of
Master in Biomedical Engineering

Supervisors:
Prof. Dr. Paulo de Carvalho (University of Coimbra)
Dr. Jens Muehlsteff (Philips Research Eindhoven)

Coimbra, 2018

This work was developped in collaboration with:

Center for Informatics and Systems of the University of Coimbra

Philips Research Eindhoven - Patient Care and Measurements

Acknowledgments

First of all I would like to start by thanking both my supervisors Prof. Paulo Carvalho and Dr. Jens Muehlsteff for the all the guidance, teachings and support given during the year. By example, you inspired me to develop my work ethic and have given me an immense opportunity to work in a real-life project, which allowed me to grow and better understand how research should be conducted, and for all this I am extremely thankful. I would also like to thank CISUC and Philips for providing me extremely fulfilling international experiences this year, further developing my interest for the research field.

For all my friends, thank you for everything. There are those of you who have sticked with me for so many years now that it almost seems like forever, and whatever distance comes up between us (as it has already), you are never really far away. For those who I have know for almost exactly 5 years now, thank you for such a wild ride. I wouldn't change any of our stupid decisions for another 5 years of life. A special shout out for everyone from Floralaan Oost. I had no idea what I had coming when I blindly booked my room, but I could not have asked for better housemates. You made Eindhoven a very warm place, even when it was freezing outside.

For Sara, thank you simply for being you. The world can be a mad jungle sometimes, but you are always able to calm my heart and my mind. Thank you for believing in me even when I can't.

Last but definitely not least, for my parents and my brother. You have put up with me literally from the moment I was born, and I would not be here without your constant support, confidence and love. Everything in my life I owe to you and words can never express the gratitude I feel for that.

"*I love deadlines. I like the whooshing sound they make as they fly by.*"

Douglas Adams

Resumo

Ataques de paragem cardíaca são hoje em dia um problema de saúde pública, responsáveis por um número substancial de mortes tanto na Europa como nos Estados Unidos da América. Apesar de as taxas de sobrevivência serem extremamente baixas, verifica-se um aumento significativo destas com a aplicação de ressuscitação cardiopulmonar. O intervalo de tempo existente desde o início do ataque até ao início do procedimento de ressuscitação, bem como a aplicação de compressões toráxicas ininterruptas são dois dos principais determinantes de sobrevivência e de complicações que possam surgir após o ataque. No entanto, ainda é necessário realizar pausas para a verificação da presença de pulso durante o procedimento, de modo a determinar se existe retorno de circulação espontânea. O método principal de avaliação da presença de pulso é a palpação manual, uma técnica que consiste na colocação de um dedo por cima de uma artéria que se encontre próxima da superfície da pele. Contudo, este procedimento apresenta várias limitações: é falível a erros, altamente subjetivo e muitas vezes moroso. Assim sendo, existe a necessidade de uma técnica de deteção e caracterização de pulso automática que seja objetiva e de confiança. Esta técnica precisa ainda de ser de fácil aplicação, de modo a evitar demoras no início ou na continuação das compressões.

O uso de um sensor de acelerómetro (ACC), colocado na superfície da pele acima da artéria carótida, surge como uma abordagem interessante para este problema. Estes sensores ainda que baratos e de baixa potência, apresentam alta sensibilidade e portabilidade.

De modo a estudar a viabilidade do uso destes sensores, num cenário de ressuscitação, foi construído um protocolo com o intuito de simular, num ambiente controlado, características presentes numa situação real. Usando-se este protocolo foi criada uma base de dados com sinais de 12 voluntários saudáveis. Para cada sujeito procedeu-se à medição síncrona de dois sinais ACC, eletrocardiograma e fotopletismograma. Adicionalmente, estava disponível uma base de dados de um

estudo prévio, composta por sinais de 5 pacientes medidos em situações reais de ressuscitação, possibilitando comparar o comportamento dos sinais simulados com os sinais reais. Usando-se estas duas bases de dados foram desenvolvidas soluções técnicas, com o uso de dois diferentes classificadores para a discriminação de artefactos, compressões, presença e ausência de pulso.

A primeira abordagem, baseada num estudo prévio, consiste num classificador em cascata que inicialmente classifica cada janela de 3 segundos com uma medida de atividade, seguidamente realizando outra classificação, esta por sua vez, com o uso de uma medida de periodicidade. Uma extensão deste trabalho foi concetualizada e implementada usando-se novas características que se baseiam no conhecimento do domínio e informação fundamental do sinal. As características foram retiradas tanto de uma representação no domínio do tempo, como da reconstrução do espaço de fase do sinal. Para determinar que características utilizar na discriminação em cada passo do classificador em cascata foi usada uma técnica de redução de características. Apesar de cada classificador individual apresentar bons resultados, a sua combinação em cascata apresentou desempenhos baixos devido à acumulação de erros, intrínseca desta abordagem.

A segunda abordagem, baseada no uso de um classificador multi-classe, revelou ser bem sucedida na melhoria do desempenho. Para este classificador, a seleção de características foi realizada testando-se todas as combinações possíveis, escolhendo-se aquela que apresentasse um desempenho ótimo. Observaram-se melhorias gerais dos resultados, com os classificadores testados nos dados simulados a apresentarem exatidões finais médias de 89% e 97%. Contrariamente, os resultados apresentados relativamente aos testes nos dados reais são piores, apresentando exatidão final média de 57%. Os desafios existentes no trabalho realizado consistem no acesso limitado de dados reais, bases de dados pequenas e o facto da anotação dos sinais ter sido realizada sem opinião clínica.

Palavras-chave: Acelerómetro, Deteção de Pulso, Ressuscitação Cardiopulmonar, Engenharia de Características

Abstract

Cardiac arrest is a major health problem accounting for a substantial number of deaths in both Europe and the United States. Despite survival rates being extremely low, delivery of Cardiopulmonary Resuscitation (CPR) has been proven to have a significant survival benefit. The interval from collapse to initiation of CPR, as well as maintaining uninterrupted compressions are two of the major determinants in the survival outcome and the complications as follow-up after the event. Nevertheless, pulse checks are still necessary interventions to assess return-of-spontaneous circulation. The Golden Standard for pulse assessment is manual palpation, a method which consists of placing a finger above an artery that is close to the skin surface. This procedure has several limitations: it is unreliable, highly subjective and often takes too long. Hence, there is a need for a reliable, objective and automatic pulse detection and characterisation technique for CPR scenarios. This technique needs to be easy to apply avoiding delays in initiation or continuation of chest compressions.

The use of accelerometer (ACC) sensors above the carotid artery, provide an interesting approach to this problem. They are characterised for being inexpensive and low power, nonetheless presenting high sensitivity and portability.

In order to study the basic feasibility of these ACC sensors in a resuscitation scenario, a protocol was designed with the aim of simulating characteristics present in a real-life scenario under controlled conditions. Using this protocol, a dataset of 12 healthy volunteers' signals was created. For each subject two ACC signals, electrocardiogram (ECG) and photoplethysmography (PPG) were measured synchronously. Additionaly, a dataset from a previous study of 5 patients undergoing real-life CPR was available allowing for a comparison between the behaviour of the simulated acquired data with real-life signals. Using these two datasets, technical solutions were developed with two different classifiers discriminating artifacts, compressions, pulse and absence of pulse.

The first approach was based on a previous study, consisting in a two-step cascade

classifier which initially classified each 3-second window based on an activity measure and followed by using on a periodicity measure. An extension of this work was conceptualised and implemented using extra features based on domain knowledge and fundamental information of the signal. Features were both extracted in a time domain representation as well as in the phase space reconstruction of the signal. A feature selection score was used to determine the features for each internal classifier of the algorithm. Despite the good results of each classifier individually, their cascade combination performance performed poorly due to accumulation of errors which is intrinsic to such an approach.

The second approach based on a sole multiclass showed successfully an improved performance. For this classifier, feature selection was performed using a wrapper approach which allowed for the selection of the combination of features which performed optimally. General improvement of the results was observed, with the classifiers tested in the protocol data showing exceptional results, with final accuracy averages of 89% and 97%. Conversely, results in the real-life data were poorer, with the final accuracy averaging 57% . Challenges in the work comprise limited access to real-life data, small datasets and annotation of the signals which was performed without medical expertise.

Keywords: Accelerometer, Pulse Detection, Cardiopulmonary Resuscitation, Feature Engineering

Contents

List of Tables

List of Figures

Abbreviations

ALS	Advanced Life Support
AUC	Area Under the Receiver Operating Characteristic Curve
AUC$_{c-curve}$	Area Under the C-Column Average Curve
AV	Atrioventricular Node
BCG	Ballistocardiogram
BP	Blood Pressure
CPR	Cardiopulmonary Resuscitation
DBP	Diastolic Blood Pressure
ECG	Electrocardiogram
EMS	Emergency Medical Services
EN	Entropy
ETCO$_2$	End-tidal Carbon Dioxide
FSS	Feature Selection Score
GE	Geometric Mean
HUTT	Head-up Tilt Table
KU	Kurtosis
LHP	Module of the lag of the highest peak in the autocorrelation
LOO	Leave-One-Out
OHCA	Out-of-Hospital Cardiac Arrest
P$_{4Peaks}$	Power of the Four Highest Peaks of the periodogram

pVT Pulseless Ventricular Tachycardia

PAT Pulse Arrival Time

PEA Pulseless Electrical Activity

PEP Pre-Ejection Period

PM Prominence

PPG Photoplethysmogram

PSR Phase Space Reconstruction

PWV Pulse Wave Velocity

ROC Receiver Operating Characteristic

ROSC Return of Spontaneous Circulation

SA Sinoatrial Node

SBP Systolic Blood Pressure

SF Spatial Filling

SK Skewness

SM Simplicity

STD Standard Deviation

$\mathbf{STD}_{acc'}$ Standard Deviation of the derivative of the ACC signal

$\mathbf{STD}_{xz}$ Standard Deviation of the correlation between axis x and z

$\mathbf{STD}_{yz}$ Standard Deviation of the correlation between axis y and z

TE Teager Energy

VF Ventricular Fibrillation

1

Introduction

1.1 Contextualisation and Motivation

The main goal of this thesis is to explore the use of low-intrusive, simple and cheap accelerometer (ACC) sensors for pulse detection in Cardiopulmonary Resuscitation (CPR) settings. For this end, an acquisition protocol was established, with the purpose of simulating expected characteristics present in a real-life resuscitation scenario, and technical solutions were built and tested in this dataset, as well as in already existent real-life data.

Cardiac arrest is a major health problem accounting for a substantial number of deaths in both Europe[6] and the United States[7]. The number of patients who suffer from OHCA (Out-of-Hospital Cardiac Arrest) annually in these two parts of the world have been reported to be approximately 275,000 and 356,000 respectively.[8][7] Despite survival rates of cardiac arrest being extremely low, delivery of CPR has been proven to exert a significant survival benefit[9, 10]. Nevertheless, quality of chest compressions, which has been observed to be sub-optimal[11], in addition to other several factors can hinder the efficiency and outcome of the resuscitation effort.

Duration of the ressuscitation is one of the major determinants already identified by previous studies. It can be defined as the sum of two distinct intervals: (1) no-flow interval , i.e. interval from collapse to initiation of CPR; (2) low-flow interval, i.e. interval from start of CPR to return of the spontaneous circulation (ROSC) or termination of resuscitation. It has been proven that there is a strong correlation between the first interval and the survival status[12]. Therefore, the longer the no-flow interval, the lower the survival rates and the worse the sequelae suffered from the cardiac event are. On the other hand, uninterrupted compressions are strongly emphasised by current resuscitation guidelines. Even short interruptions to chest compressions can prove disastrous for outcome and every effort must be

made to ensure that continuous chest compressions are maintained during the resuscitation attempt, making only brief interruptions for specific interventions, such as pulse checks. Manual pulse palpation is still the Golden Standard for assessment of pulse presence in unconscious patients for professional rescuers[13]. However, this method presents some challenges, which consequently also affect the efficiency of the resuscitation process. One of the major challenges in palpation is that pulse detection takes too long(often 25s or more[14, 15, 16]) and is very unreliable as well as highly subjective, with a reported sensitivity of 90% and specificity of 55%[17]. Nonetheless, pulse detection is still perceived by the resuscitation community as a fulcral technique for the assessment of the need for CPR in an emergency situation and is recommended for Advanced Life Support (ALS) rescuers[13]. Therefore, a need for a reliable, objective and automatic pulse detection and characterization technique for CPR scenarios can be identified. Such a technical solution should also be characterised by ease of application on the patient and use by emergency medical services (EMS) personnel, thus improving the responsiveness and the efficiency of the resuscitation process.

Accelerometry presents itself as a technology which offers great interest and promise for this end. Accelerometer sensors are inexpensive and low power, nevertheless presenting high sensitivity and portability, which make for the detection of pulses readily possible[1, 18]. Thus, the aim of this thesis is to explore the use of accelerometer sensors as an information source for the development of reliable and viable mechanisms to support resuscitation techniques.

1.2 Thesis Structure

The current document is divided into the following chapters:

Chapter 2 - Physiological and Measurement Background - description of all the physiological background required for understanding the work developed.

Chapter 3 - State of the Art - where previous developed work related to accelerometry and cardiopulmonary resuscitation is presented and assessed with respect to limitations and challenges.

Chapter 4 - Experimental Setup and Study Protocol - description of the experimental setup used for the data acquisition process. The protocol designed is explained with a brief data analysis presented for the two different datasets. Annotation of the measured signals is also discussed.

Chapter 5 - Pulse Detection using Accelerometer Signals from the neck area with carotid artery underneath - feature engineering and the approaches developed for automatic classification of four different classes present in CPR scenarios are discussed. Results are obtained using a Leave-One-Out validation, with tests being performed independently on each dataset.

2

Physiological and Measurement Background

In this chapter, all the concepts concerning the Physiological and Measurement Background necessary for a correct understanding and elaboration of the research work are presented.

2.1 Cardiovascular System

The cardiovascular system is a system of vital importance in the human body, consisting of three interrelated components (heart, blood and blood vessels). It permits the transportation of oxygen, carbon dioxide, nutrients and hormones to and from body cells without which all the different organ systems present in the human body could not function. It is also a major contributor to the regulation of the body pH and temperature as well as playing an active role in the immune response[3].

Blood, one of the three interrelated components of the system, is the body fluid in which several substances are transported throughout the body. It is also responsible for the regulation of several life processes and for protection against external factors. The heart, on the other hand, is the muscular organ responsible for pumping the blood allowing circulation through pressure gradients. The circulation occurs in an unidirectional way through the blood vessels, the final component of the system. These provide the structures necessary for the flow of blood to and from the heart, each vessel belonging to one of two different interconnected circulations: the pulmonary circulation and the systemic circulation. In the former, blood from all regions of the blood is pumped from the the right ventricle into the pulmonary trunk, arriving at the lungs where carbon dioxide present in the blood is released and oxygenation occurs. Afterwards, it returns to the heart where the systemic circulation

begins. Blood reenters through the left atria, passing into the left ventricle and it is pumped to all the body tissues. Here it releases different materials necessary for the cells normal functionality (e.g. oxygen, hormones and nutrients) and receives cell waste, such as carbon dioxide, returning to the heart through the right atria, once again restarting the cycle[3][2].

It is important to note that deoxygenated blood, i.e., the blood circulating in the pulmonary circulation, is called venous blood, while the blood circulating in the systemic circulation is named arterial blood.

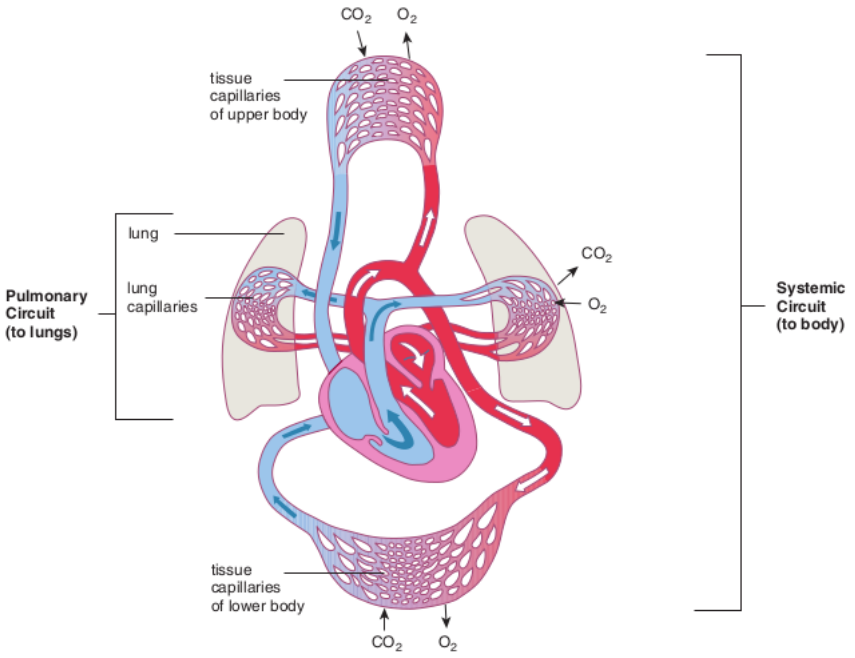

Figure 2.1: Pulmonary and Systemic circulations. Right side pumps venous blood through the pulmonary circulation, whilst the left side sends arterial blood through the vessels of the systemic circulation[2]

When exiting the heart, the blood is sent through arteries, blood vessels which present thicker muscular walls as to withstand the higher values of pressure caused by the blood flow. After travelling through the body, it returns to the heart in veins, vessels which are less muscular than arteries. In most veins, valves are also present in order to prevent backflow of the blood[2].

2.1.1 The Heart (Cardiac Cycle)

The heart is a muscular organ, located near the midline of the thoraxic cavity, between the lungs with about two thirds of its mass lying to the left side of the

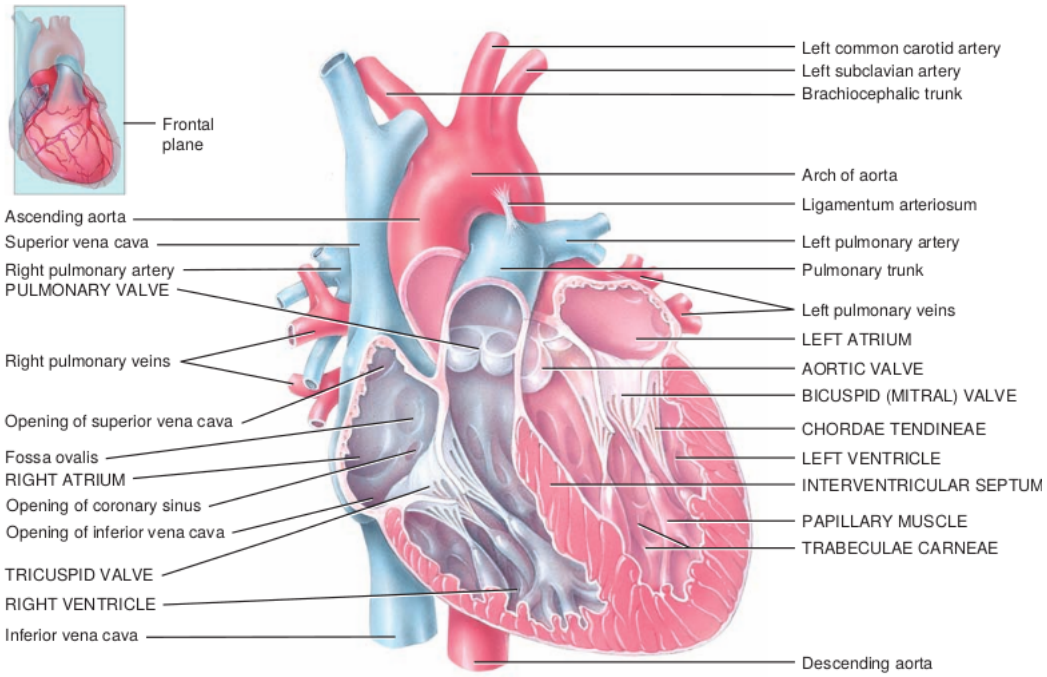

Figure 2.2: Internal anatomy of the heart. Right side depicted blue to represent the flow of venous blood and left side red for representation of arterial blood flow [3]

body[3]. As is depicted in Figure 2.2, the heart is divided into 4 separate chambers, two atria(superior chambers) and two ventricles(inferior chambers). Internally, the atria are separated by the interatrial septum and the ventricles by the interventricular septum, thus meaning that the heart is divided in a right and left side. The thickness of each chamber's myocardium (the muscle component in the heart wall) is adjusted to its function. On one hand, the atria which receive blood in the heart and send it into the adjacent ventricles, have thin walls. The ventricles however, having to pump blood to parts of the body have thicker myocardium. The left ventricle, being involved in the systemic circulation and having to send blood to all body has a thicker wall than the right ventricle which is involved in the pulmonary circulation. Other structural components involved, which play an important role in the unidirectional flow are the valves. The mitral and triscupid valves are located between the atria and the ventricles, preventing blood from returning to the atria when pumped into the ventricles. The pulmonar and aortic valves prevent return of the blood to the heart after being pumped into the arteries[3][2].

The heart's contraction and relaxation movements are efficiently controlled by a system of electrical stimuli originated from specialised cardiac muscle fibers: autorhythmic fibers. By providing a path for each cycle of cardiac excitation to progress in

the heart, it ensures that the chambers contract in a coordinated manner.[3] The conduction system is an intrinsic one, meaning there is no need for external nervous simulation in order for the heart to beat. Nodal tissue, i.e., tissue with both nervous and muscular characteristics, is then responsible for the heartbeat. It is found in two regions of the heart: located in the upper posterial wall of the right atrium is the sinoatrial node (SA), and in the base of the right atrium close to the septum is the atrioventricular node (AV)[2]. The SA is called the pacemaker as it plays a vital role in keeping the hearbeat regular.

All events which occur during one heartbeat constitute the cardiac cycle. Although there are separate sides of the heart, the contraction events occurs simultaneously. First the two atria contract, followed by the contraction of the two ventricles. As there are movements of contraction, or systole, there also movements of relaxation called diastole. It is this cycle of coordinated and efficient movements that allow the effective circulation of the blood through the heart and body[2].

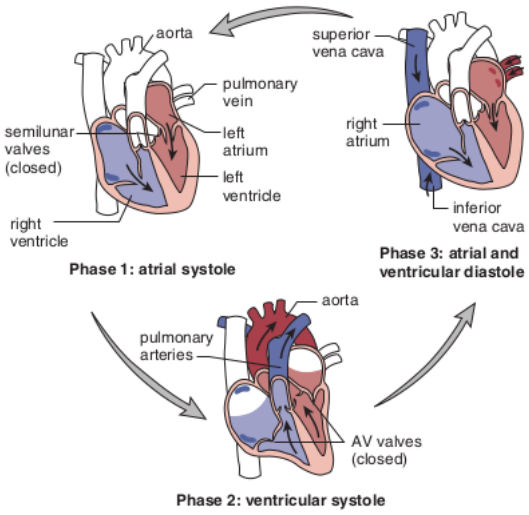

Figure 2.3: Stages in the cardiac cycle[2]

2.2 Blood Pressure Regulation

Atria and ventricles' movements of contraction and relaxation create pressure gradients which allow blood flow to occur. The blood flows from regions of higher pressure to regions of lower pressure with blood flow directly proportional to the pressure difference. Blood pressure (BP) is the pressure created by the blood flow against a blood vessel wall[3]. As show in Figure 2.4, systemic blood pressure (SBP)

decreases progressively with distance to the left ventricle. It reaches its lowest value in the venae cavae because they are farthest from the left ventricle.

As can be observed in Figure 2.4, blood pressure fluctuates between systolic blood pressure and diastolic blood pressure (DBP). The former corresponds to the pressure against the arterial walls after a left ventricle contraction, whilst the latter corresponds to the pressure before the left ventricle contraction. In the systemic circulation the expected BP oscillates 120 mmHg (SBP) and decays to 80 mmHg (DBP), while in the pulmonary circulation SBP is approximately 25 mmHg and DBP 10 mmHg[2].

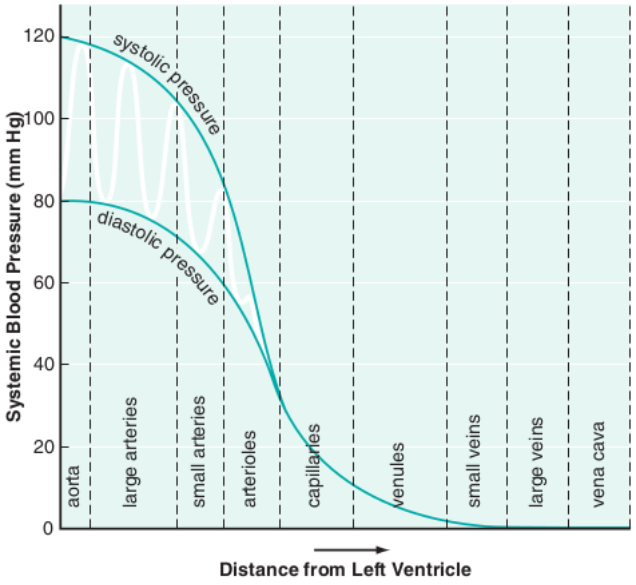

Figure 2.4: Blood Pressure during systemic circulation[2]

Different physiological factors can lead to changes in arterial blood pressure. These include heart rate, cardiac output(volume ejected from the heart per unit of time) and venous return(blood volume which flows back to the heart). Blood viscosity and peripheral resistance(the friction between the blood and the walls of vessels) also affects blood pressure, with greater resistance leading to greater BP[19].

Blood pressure regulation is dependent on the interconnection of the nervous and endocrine systems which cause fluctuations in numerous physiological aspects such as the ones mentioned above. These variations allows the body's performance to be optimised to the different conditions and scenarios to which it is exposed[3][2].

2.3 Electrocardiogram and Photoplethysmography

An Electrocardiogram (ECG) is the recording of the electrical signals, generated by the action potentials propagation through the heart during a cardiac cycle. In a typical recording it is possible to observe three characteristic waves, each relating to a moment of the heart's cycle: The P wave, the QRS complex and the T wave (see Figure 2.5). The P wave represents atrial depolarization, while the QRS complex represents the rapid ventricular depolarization. Finally the T wave represents ventricular repolarization, occuring just as the ventricles are starting to relax[3].

Analysis of the ECG allows for extraction of several diagnostic and prognostic factors which reflect the cardiac condition, thus proving useful in a wide range of applications[20][21]. However, ECG-only analysis has its limitations and for a better understanding of relevant cardiac function and hemodynamics variables present it is necessary to use signals-fusion techniques, extracting some values such as the pre-ejection period(PEP) or the pulse arrival time(PAT).

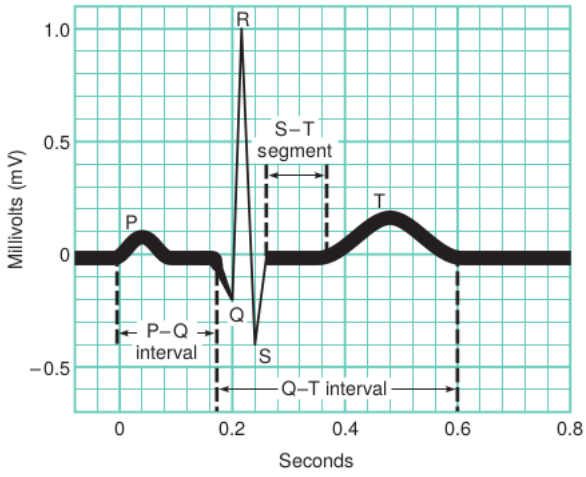

Figure 2.5: Normal representation of ECG with reference points[3]

A Photoplethysmogram (PPG) is an optical measurement technique which uses a light source(invisible infrared light) and a photo-detector[4]. The PPG signal reflects the cardio-vascular pulse wave that propagates throught the blood vessels by measuring the amount of backscattered light which corresponds to the variation of the blood volume[4, 22, 23]. The signal can be divided into a systolic wave and a diastolic wave, as seen in Figure 2.6. Despite the wave countour's simplicity several physiological important features can be extracted such as the pulse rate, left ventricle ejection time, stifness index and reflection index[22]. As inflections can prove hard to detect in an original PPG, the PPG's first and second derivative are

also commonly used.

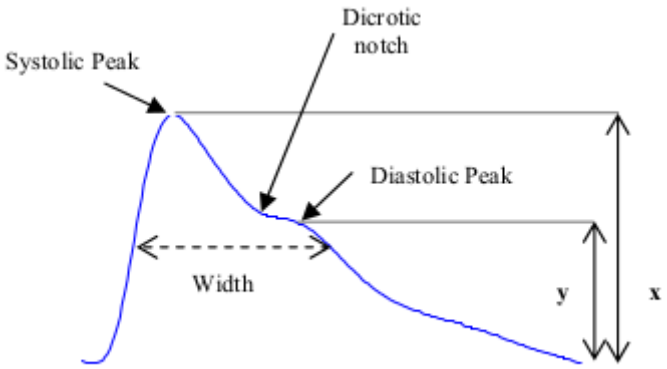

Figure 2.6: Normal representation of a PPG wave[4]

2.4 Carotid Pulse

In the aortic arch, the continuation of the ascending aortha, there are three major arteries which branch out. As visible in Figure 2.7 these are the brachiocephalic trunk, the left common cartery and the left subclavian. The brachiocephalic trunk will then further branch out into the right common carotid artery and the right subclavian artery. Each of the carotid arteries will separate in an internal and external artery, being responsible for the supply of blood to the face, eyes, neck and brain[3].

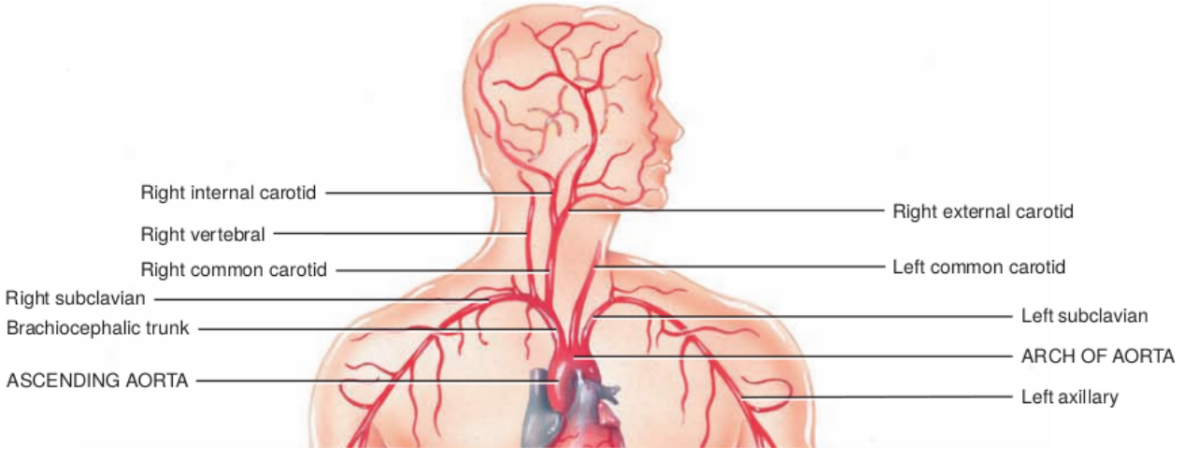

Figure 2.7: Some of the major arteries and its branches[3]

The expansion and recoil of elastic arteries occurring with alternation after a systole of the left ventricle generates a traveling pressure wave. This wave is denominated

pulse, and is strongest in the arteries closest to the heart due to the loss of pressure when blood is flowing through the vessels. It can be felt in several arteries that lie near the surface of the body, such as the carotid artery[3]. In this case, the pressure wave observed is called carotid pulse and it can present a specific morphology characterised by a smooth, relatively quick upstroke and a smooth, more gradual downstroke[24]. The pulse rate is normally the same as the heart rate[3], and in literature pulse presence is considered when an attainable pulse in the carotid measures 60 mmHg or higher[1].

2.5 Cardiopulmonary Resuscitation

Cardiopulmonary resuscitation is the procedure employed in case of cardiac arrest. In such an event survival rates are very low[6][7] even when CPR is employed. However, this method does improve the possibility of achieving ROSC[8][9][10]. It is vital that the response is quick and effective, starting CPR as soon as possible in order, as the no-flow period(the amount of time between the cardiac event and the start of CPR) has been proven to demonstrate correlation with the survival rate[12]. Through the execution of chest compressions in an uninterrupted manner, with the appropriate depth and rate of around 100-120 bpm, blood perfusion to the heart and brain is attainable. Performance quality of the procedure, subjectivity of certain associated procedures and yet not completely understood physiology are some of the factors with hinders CPR's efficiency and leave to wonder that there is still room for further development and improvement of the method[25].

Chest compressions move blood during cardiac arrest and the resuscitation by two distinct mechanisms identified as the cardiac pump and the thoracic pump. In the first mechanism a forward blood flow from the left ventricle is generated by the external chest compressions causing the heart to be squeezed between the sternum and the spine. The second mechanism operates due to a global rise in intrathoracic pressure which is observed during the chest compressions. This rise is sufficient to create a blood flow from the pulmonar blood vessels to and through the heart and into the periphery[26].

Two different heart rhythms are associated with scenarios of cardiac arrest: shockable rhythms and non-shockable rhythms. Despite the ALS cardiac arrest algorithm being applicable to all scenarios of cardiac arrest, understanding the individual situation present allows for the performance of additional interventions[13].

2.5.1 Shockable rhythms

When observing the heart rhythm using an ECG, the first monitored rhytmn in about 20% of both in-hospital and out-of-hospitals cardiac arrests, is a shockable rhytmn, meaning it corresponds to ventricular fibrillation(VF) or pulseless ventricular tachycardia(pVT). In such a scenario there exists the possibility of using an electrical defibrillator which highly increases the survival prospects of the resuscitation effort. However chest compressions still play an important part in the resuscitation procedure and should be commenced as soon as cardiac arrest is confirmed and only interrupted in between for the shocks and other necessary interventions. Even a slight delay between the pausing of the chest compressions and the delivery of the shock(preshock pause) can reduce the chances of survival[13].

2.5.2 Non-shockable rhythms

There exist two observable non-shockable rhythms, pulseless electric activity(PEA) and asystole. PEA is present when the ECG presents electrical activity which would normally be associated with a palpable pulse. Patients displaying this condition often have mechanical myocardial contractions, but these are not strong enough to produce detectable pulse or blood pressure. Thus the ECG alone, does not allow for pulse assessment and it is for this reason that pulse checks are still a necessary procedure during CPR. Asystole on the other hand corresponds to the lack of electrical activity from the heart. These conditions are often present due to reversible causes, and survival following cardiac arrest when non-shockable rhythms are displayed is unlikely unless the reversible cause is found and treated[13].

It is also important to remark that even though initially a non-shockable rhythm can be observed, this one can transition into VF/pVT at some stage during resuscitation, in which case defibrillation can be attempted.

2.6 Accelerometer Signal on the Carotid Artery

Accelerometers are small sensing devices that measure the acceleration applied to the sensor, thus also measuring the accelerations applied to the body to which the sensor is attached. They are already found in use in a great number of consumer applications and nowadays an accelerometer sensor which is small, inexpensive and low power presenting high sensitivities, is easily available[27].

On the focus of this thesis, by applying an accelerometer attached to the skin above the underlying carotid artery, it is possible to measure a pulse signal[27]. When the heart ejects blood it creates a pulse pressure wave which causes the dilatation of the artery's wall, consequently generating an acceleration. As depicted in Figure 2.8, along with the pulse signal, the sensor will also measure the gravitational acceleration component, noise (i.e., all artifacts from moving, swallowing, talking, etc), along with physiological signals[28].

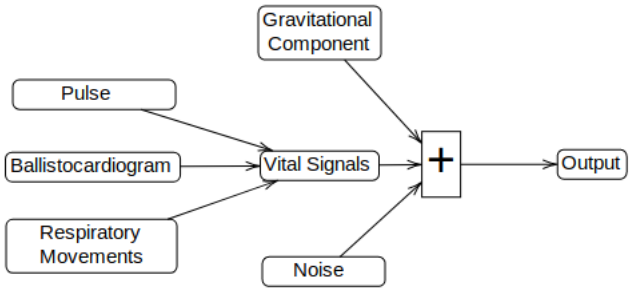

Figure 2.8: Components of the accelerometer signal obtained at the carotid

The gravitational component corresponds to the offset of the different axes which can be observed during moments of static conditions, or during steady state non-rotational movement. This components allows for the determination of the sensor's orientation relative to the vertical plane. This knowledge can be interesting from a signal processing perspective as it allows to compare changes of position by the gravitational component and changes in signal morphology[28].

Besides the pulse signal some other physiological signals appear in the obtained signal, such as the ballistocardiogram (BCG) and respiratory movements. The former is observed because of the vibrations created by the heart momentum when ejecting blood. The latter is observed due the thoraxic movements existent during the respiratory cycle[29]. These generate vibrations on the body which logically create an acceleration which is also measured with the sensor. While these signals can be of interest for signal fusion approaches, in order to optimise algorithms it is important to understand how one can supress its influence if necessary.

Noise in the signal can appear from several body functions and motion artifacts[30]. Examples can be: swallowing, neck movements, arm movements, rotation, among others. These can complicate the extraction of the desired vital signal parameters which consequently compromises the utility of accelerometers in healthcare scenarios.

2.7 Conclusion

This chapter aimed both to introduce the physiological background necessary for the complete understanding of the work developed in this thesis, as well as to explain and contextualise the cardiopulmonary resuscitation procedure and the signal which is to be expected when using an accelerometer in the carotid artery for medical applications.

3

State of The Art

In this chapter, the focus will be on showing current uses of accelerometers, explaining how such a sensor presents a wide array of possibilities and how it can apply to pulse detection and characterisation. Present literature regarding cardiopulmonary resuscitation and its advantages, disadvantages and challenges for future works will also be discussed.

3.1 Accelerometry

Accelerometers have already found widespread use in several consumer applications, particularly tablets, smartphones but also wrist watches[31]. Consequently, there exists a high volume of literature regarding their use and processing analysis. Their size and low-cost permits its incorporation in a wide range of other uses and they have been recurrently studied as major components of Body Sensor Networks(BSN)[32]. These sensing networks have emerged as a revolutionary technology in many application domains such as fitness, health-care, smart cities and many other compelling Internet of Things(IoT). The technology is transitioning to multi-device synchronous measurement environments using data-fusion to directly impact application perfomance[32].

3.1.1 Activity Recognition Applications

Accelerometry based activity recognition is one of the main areas of study with several different potential applications. Chung *et al.* in [33] used a data-fusion approach of an ECG signal and a tri-axial accelerometer signal to develop a signal monitoring and analysis method for the homecare of elderly persons or patients. In their prototype application ECG is used for extraction of physiological related features, whilst the accelerometer provides feedback on the activity being performed,

specifically running and walking. Curone *et al.* in their paper[34] also use ECG and one accelerometer data for development of a device which aims to recognise activities in rescuers. Using this data features are extracted to differentiate between physical activities, intensities and postures. The aim is to identify potentially dangerous states in the rescuers such as "subject motionless lying down" or "subject resting with abnormal heart rate". Their routine was tested in data recorded on seven healthy adult subjects performing activity in laboratory settings, meaning that, despite the adequate results obtained further studies are necessary to validate the model. A different approach was taken by Tapia *et al.*[35] which combined a wireless heart rate monitor and five accelerometers not only for recognition of physical activities, but also their intensities. They used data from 21 people obtaining a recognition accuracy performace of 96.4% using subject-dependent training and 56.3% using subject independent training, thus showing that uniformization of data proves to be a challenge in itself. They also aimed to show the effect on the results when adding the heart rate data. Improvements were low with subject-dependent recognition accuracy improving by 1.2% and subject-independent accuracy by 2.1%. Wang *et al.*[36] opted for the development of a Hidden Markov Model-based recognition method, aiming to classify between six human daily activities using only data from a single waist-worn tri-axial accelerometer. The results obtained were very optimistic with the classifier demonstrating a good generalisation capacibility, whilst having low computational complexity. This raises the idea that use of feature learning techniques for feature extraction can be an interesting solution for the process of feature engineering with ACC signals. Regardless data used for training and testing consisted of uncontaminated segments of each activity and data was acquired from few subjects with low variability in age and health conditions.

3.1.2 Extraction of physiological parameters

Healthcare applicability of accelerometers is varied with literature found studying the potential use in a range of different problems[32]. Phan *et al.*[37] use an accelerometer attached to a belt around the chest for measurement of cardio-respiratory activity. The respiratory waveform is calculated using the inclination of the chest accelerometer, presenting a slow periodic variation(< 1 Hz) with weak amplitude. It is important to note that this waveform is easily mixed with body movements. The heart rate is based on the detection of the vibration peaks measured by the accelerometer in the chest, with the challenge that the vibration shape varies among individuals. Nevertheless, in a still vertical or horizontal posture re-

sults were positive, with the accelerometer signal showing potential for identification of arrhythmia or respiratory malfunction. Another potential use was analysed by Morillo *et al.*[38], which presented a body-fixed-sensor-based approach to assess potential sleep apnea patients. Different signals were retrieved synchronously, with an accelerometer placed in the neck being used for extraction of both respiratory rate and snore pitch information. The respiratory component was compared to the airflow signal acquired from a polysomnography thermistor, presenting a strong correlation with it. As many algorithms in the literature in this topic are based solely on the airflow, this result is quite interesting and further studies are required. Concerning the detection of pitch, which was benchmarked against the pitch measured by an high quality microphone, although it lead to promising results, it is not a trivial challenge and some limitations were found. During long-time apnea episodes the ACC signal recorded information which contaminated the pure snoring components. This fact, allied to the pseudoperiodicity characteristics of snores leads to an increase in complexity of the problem.

Ballistocardiograms and seismograms signals can also be measured by use of an accelerometer attached to the skin. Inan *et al.*[39] on a review regarding these methods presents different wearable applications using accelerometers.

Several limitations are present when using accelerometers in healthcare applications. Due to their high sensitivity, these sensors are highly prone to artifacts. Silva *et al.* in [30] developed a simple threshold algorithm for artifact detection in ACC signals. After performing feature extraction and selection it was found that just by using the energy of the signal it was possible to achieve interesting results in artifact reduction. However, as in other studies, the dataset was limited, with future validation in extended datasets being necessary for definitive conclusions. The threshold established was also optimised for the existent data which presented high-amplitude artifacts, with the author inferring that with different datasets the value could suffer alterations.

Another limitation which must be considered is the heterogeneous signal morphology present when using accelerometer sensors. The signals acquired are highly dependent of the positioning, thus the algorithms used have to reflect this problem. Atallah *et al.* [40] analyse this limitation regarding activity monitoring in wearable applications, studying how sensor positioning can affect identification of different activity types. Their results show that the correct choice of position(depending on the final aim) is reflected on the classification results achieved.

3.2 Cardiopulmonary Resuscitation

Cardiopulmonary resuscitation has recurrently been studied in literature. Being an important procedure for achieving ROSC after cardiac arrest, and with its efficiency and responsiveness directly correlated to the sequelae observed after a cardiac event it is vital to attain a better understanding of the topic and explore possibilities which provide improvement to the already existing guidelines, thus improving survival rates which remain low[6][7]. Objects of study are quite varied including assessment of the quality of chest compressions[11], review on existent techniques and devices for improvement of quality of care [25] and development of new methods (automatic or not) for pulse detection. The latter is the focus of the thesis and so works presented will mainly relate to this objective.

Manual palpation is still the Golden Standard for assessment of pulse, despite being prone to error and being relatively time consuming. In order to achieve better survival rates no-flow interval and interruptions in chest compressions should be minimal, thus existing a need for improving detection of ROSC in unconscious, pulseless patients[1].

In the literature studied the only commercially available solution found for pulse assessment was the CardiAid, CPR Check(California, United States). It works by using a resonant non-linear inductive-capacitive sensor to track both pulse and respiration. The pulse wave and the respiration lead to a variation in the surface of the tissue that affects the resonance circuit. allowing for the acquisition of an electrical signal and consequently its monitoring [41]. Aarts *et al.* in [31] performed a basic feasibility study to compare the performance of an accelerometer based pulse detection approach versus the CardiAid. Both approachs aimed to detect *Motion* or in the lack of it, *Pulse* or *No Pulse*. The accelerometer approach presented better sensitivities, ease of placement and the decision time for the classifier was lower. However, it is important to note that it presented limitations in the aspect that data used for comparison is from healthy subjects therefore, data regarding absence of pulse was not present.

The potential of PPG for pulse monitoring during CPR was studied in a porcine study by Wijshoff *et al.* [42]. Data consisted of PPG and arterial blood pressure, measured directly from the pigs' nose and from the aortic arch respectively. In this work by observation of the PPG time traces and the frequencies spectrograms it was possible to infer pulse presence, demonstrating that this approach shows promise for the future. However, it is important to note that this study presents some

limitations. The data is collected from animals and the PPG signals are measured from the nose, which does not represent a good clinical practice. Hence, it is not possible to directly transpose these results for clinical cases.

End-tidal carbon dioxide($ETCO_2$) measurement is an estabilished method for monitoring circulation during cardiopulmonary resuscitation. The measured signal depends on cardiac output and blood flow during the return of the blood to the heart in the pulmonary circulation, thus reflecting CPR quality and allowing prediction of ROSC[43]. Lui *et al.* in their paper[44] aimed to evaluate the diagnostic accuracy of an abrupt and sustained increase in the $ETCO_2$ values for indication of ROSC. Their results showed a sensitivity of 33% and a specificity of 97% which despite showing a potential in the scenario, require improvement. Results might also be influenced by class imbalance as they had 117 "No ROSC" events compared to 60 "ROSC" events. Information on temporal behaviour is also lacking in the article[43].

Other pulse monitoring methods include bioelectrical, ultrasonography, bioleletrical impedance and sphygmomanometry, however, all of the existing techniques mentioned present some limitations particularly regarding to size, cost, accuracy and ease of application in a resuscitation scenario. Accelerometers present an interesting approach for CPR scenarios diminishing some of common limitations having high sensitivity, portability, ease of application and low cost[1].

Muehlsteff *et al.*, having previously showed basic feasibility of the use of the accelerometer signal on the carotid for pulse presence and pulse strength assessment[27], developed an algorithm for pulse presence tracking using the data of 27 patients submited to head-up tilt-table(HUTT) test[18]. The ACC signal is transformed into a waveform which presents a similar look to that of a PPG using a proprietary algorithm. From this signal features are extracted from the peaks whilst an "activity" level is also calculated based on the variance of the ACC signal. These features are fed into a selectable(either Linear or Support Vector Machine) classifier, which will then classify each 10 second window into *Pulse*, *No Pulse* or *Motion*. It was observed that the placement of the accelerometer at the carotid artery compromises signal quality for pulse assessment in conscious individuals as it is very suscetible to motion artifacts. Nevertheless, in scenarios where motion is diminished or inexistent, pulse presence was accurately monitored. Seen that in CPR scenarios motion is more limited, this approach might exhibit potencial for pulse detection during resuscitation. Silva *et al.* developed an algorithm for pulse presence/absence classification using a simple feature based on the correlation between synchronous measurements of ECG and ACC signal on the carotid[45]. Despite the results attained being promising, it

is important to notice that the dataset used was of HUTT patients, and the pulse absence segments were introduced artificially in the signals as this segments were not present originally. These were simulated by attaching the sensor to the back of the hand where no pulse is detected. This however does not necessarily represent a real life scenario.

On a more direct approach to the resuscitation scenario Dellimore *et al.* in their study[1] developed an algorithm for pulse presence tracking, using data from patients undergoing CPR. Their approach consisted in a two step classification. First activity based classification was performed and posteriorly periodicity based classification, attributing to each 3 seconds window a label of *Pulse*, *No Pulse*, *Compression* or *Artifact*. Activity classification generally performed with high sensitivity and specificity and the compression periodicity classification also yielded acceptable results. On the other hand, pulse periodicity classification produced variable results across the different subjects, with further improvements being necessary. It is important to note that the data set was very limited with only 5 patients. Also an important remark is that results presented were not based on automatic classifiers but on patient specific thresholds, which also influences the results.

3.3 Conclusions

In this chapter an overview on accelerometry applications was discussed as well as a review on cardiopulmonary resuscitation approaches. Challenges and limitations were presented, in order for a better understanding of the difficulties present in this work.

4

Experimental Setup and Study Protocol

In this chapter all the work regarding the data acquisition process will be presented. The two datasets used in the work will be introduced. Annotation of the data and its analysis, including challenges and limitations faced will also be discussed.

4.1 Introduction

Cardiopulmonary Resuscitation is an important procedure and it should be promptly started in case of cardiac arrest or unconsciousness[13]. In the aim of this thesis to study the use of an accelerometer attached above the carotid for pulse detection during CPR, it was necessary to develop a protocol for simulated data acquisition as it was not feasible to perform real-life acquisition. The objective of this protocol was to simulate expected characteristics from a real-life scenario in a laboratory setting, thus allowing for data exploration and feature engineering with more control and knowledge. Additionally, data from a previous study[1] composed of 5 patients undergoing CPR in an hospital setting was made available, allowing for a comparison between the two datasets and providing a more realistic insight into the problems present in a real-life scenario.

4.2 Simulated Data Acquisition

4.2.1 Experimental setup

Accelerometer signals in a controlled study with subjects mimicking CPR phases were acquired using the SENSATRON device. This multi-parameter battery oper-

ated device (Figure 4.1) was developed by Philips[5] and allows synchronous measurement of ECG, impedance cardiography, near-infrared PPG, infrared PPG, thoracic inductive plethysmogram, sound signals and up to three tri-axial accelerometers.

Figure 4.1: SENSATRON device and its components, central unit, battery and charger[5]

In this work, the device was used for measurement of ECG, PPG and two accelerometer signals. Sound signals were also retrieved as during the acquisitions an external loud noise was made to support the annotation of the data. Sampling rates vary with the ECG being extracted at 250 Hz, PPG at 62.5 Hz, sound signals at 4000 Hz and ACC signals at 125 Hz. All signals are acquired with 16 bit ADC resolution. In this work only the accelerometer signal is used. However, emphasis was put on designing a protocol from which the data acquired can be used for future investigation of other hypotheses as well.

Data acquisition was performed with the subject lying down on an air mattress, with the two accelerometers positioned above the left external carotid artery. As seen in Figure 4.2 one accelerometer was positioned above the other, with pulse being palpable in both positions chosen.

The study was approved by the Ethics Committee of the Faculty of Medicine of the University of Coimbra.

4.2.2 Protocol

To test and develop algorithms a data collection study was performed with 12 healthy volunteers (Table 4.1). The protocol was designed to simulate typical phases and artifacts present during a resuscitation event. During CPR some body movement, although brief and stochastic are expected. On the one hand, intensity of

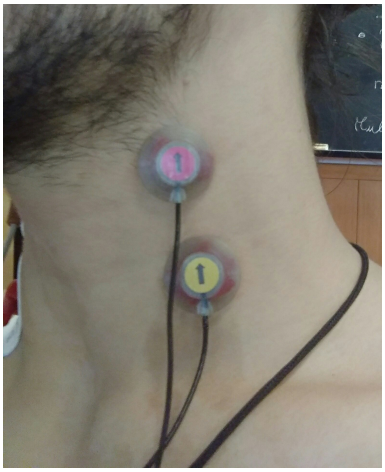

(a) Example of the positioning of the two sensors

(b) Acquisition setup

Figure 4.2: Experimental setup

chest compressions can lead to whole body movements and on the other hand the rescuers' intervention can also lead to motion artifacts being present in the signal. Since the accelerometer is positioned in the neck area, and patients are lying down during the intervention the body members whose movement more directly affects the ACC signal obtained are the neck and the arms. Thus, the protocol consisted of six distinct phases, specifically: lying down, neck movements, arm movements, compressions, compressions with neck movements, compression with neck and arm movements. Each phase had a duration of 30 seconds and the transitions in between had variable length. An outline of the protocol implemented can be observed in Table 4.2.

As it is not safe nor recommended to apply chest compressions in a healthy person, compressions are applied at the subject's chest level on the air matress. By generating a fluctuation on the mattress at the normal compression rate(100-120 compressions per minute), the subject will also oscillate and a periodical component at the adequate rate of compression will appear in the signal.

Table 4.1: Biometric information of the healthy volunteers

# of Subjects	Age [years]	BMI [kg/m^2]	$\Delta_{accelerometers}$ [mm]
12	22.750 ± 0.866	21.899 ± 1.691	32.750 ± 3.793

Table 4.2: Outline of the protocol

$t_{beginning}$	t_{end}	Phase	ECG
00:00	00:10	Transition	Yes
00:10	00:40	Lying Down	Yes
00:40	00:50	Transition	Yes
00:50	01:20	Neck Movements	Yes
01:20	01:30	Transition	Yes
01:30	02:00	Arm Movements	Yes
02:00	02:10	Transition	Yes
02:10	02:40	Compressions	Yes
02:40	02:45	Transition	Yes
02:45	03:15	Compressions with Neck Movements	Yes
03:15	03:20	Transition	Yes
03:20	04:10	Compressions with Neck and Arm Movements	Yes
04:10	04:40	Lying Down	Lose cable
04:40	04:50	Transition	Unstable
04:50	05:20	Neck Movements	Unstable
05:20	05:30	Transition	Unstable
05:30	06:00	Arm Movements	Unstable
06:00	06:10	Transition	Unstable
06:10	06:40	Compressions	Unstable
06:40	06:45	Transition	Unstable
06:45	07:15	Compressions with Neck Movements	Unstable
07:15	07:20	Transition	Unstable
07:20	07:50	Compressions with Neck and Arm Movements	Unstable
07:50	08:10	Transition (BCG)	Unstable
08:10	08:40	Lying Down	Unstable
08:40	08:50	Transition	Unstable

Considering the aim of testing other hypotheses with this dataset in future works, in the penultimate transition phase of the protocol the bottom accelerometer was transfered to the forehead allowing for the extraction of a BCG signal. Initial feasibility tests on the use of Independent Component Analysis methods were involved in the decision of extracting this signal.

In Figure 4.3 it is possible to observe one example of the two acceleration signals measured synchronously by the two sensors from one run of the simulated protocol.

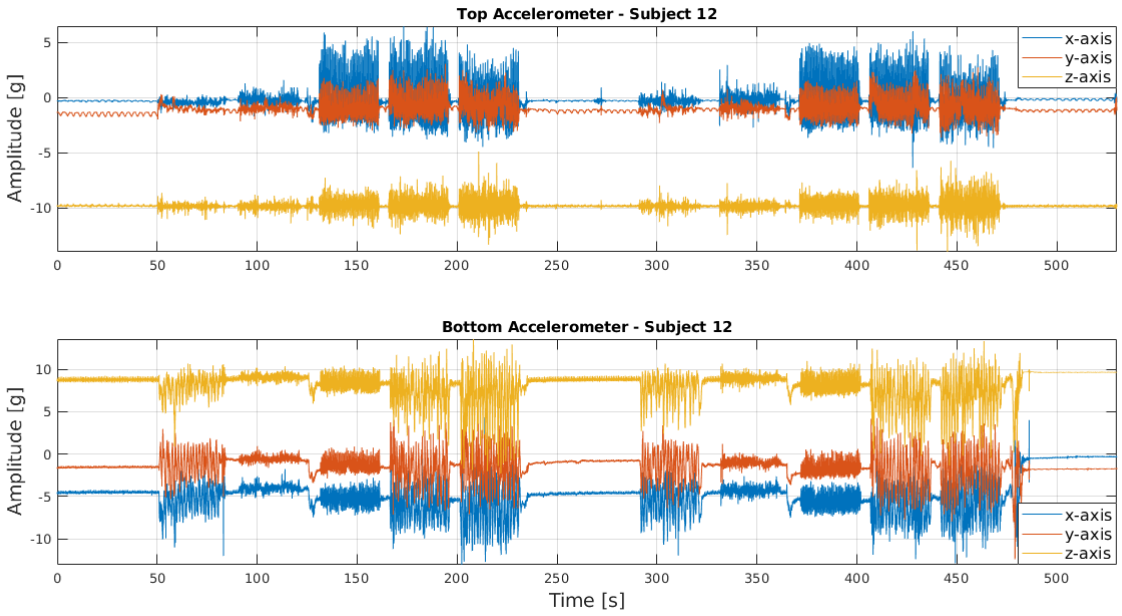

Figure 4.3: Example of unfiltered accelerometer signals obtained in the simulated data acquisitions. Upper diagram shows tri-axial ACC signal obtained from the top accelerometer. Lower Diagram shows tri-axial signal obtained from the bottom accelerometer

4.3 Data Analysis

Understanding challenges and limitations of the protocol established and the sensing modality used is vital for a complete understanding of the results obtained and future developments in the area. It is also important to observe how the protocol data behaves in order to compare the simulation to the signal obtained in a real life CPR scenario. Certain frequency characteristics are expected, shown in Table 4.3.

Table 4.3: Assumed frequency characteristics of Pulse and Compression

	Rate Interval	Frequency Interval
Pulse	60 - 100 [bpm]	1 - 1.66 [Hz]
Compression	100 - 120 [cpm]	1.66 - 2 [Hz]

One of the major limitations faced when using an ACC sensor is that the morphology of the signal measured is very dependent on the positioning of the sensor. This can be observed visually in Figures 4.4, 4.6 and 4.7, where it is clearly observable that the signal measured by the top accelerometer is more contaminated by artifacts.

For one, the pulse peaks are not as prominent in the signals from this sensor location as they are in the bottom accelerometer(Figure 4.4). This visual observation is

corroborated by the frequency analysis of the 10 second window depicted in Figure 4.4. In Figure 4.5 it is possible to observe that the fundamental frequency of the pulse signal and its harmonic (visible in the periodogram of the ECG) are more present in the bottom accelerometer, whilst in the top accelerometer other frequencies contaminate the signal.

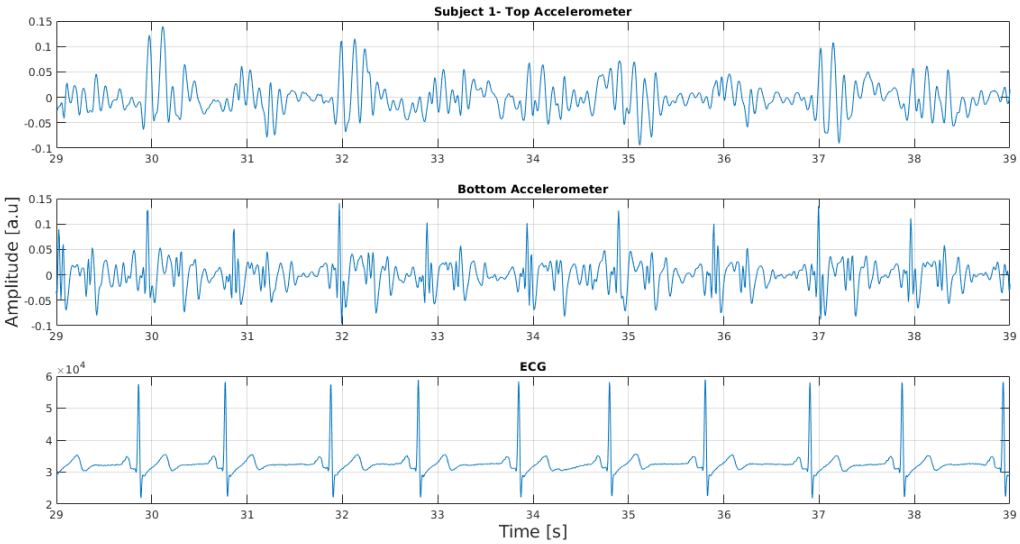

Figure 4.4: Example signals for subject 1- Upper diagram: Signal measured by the z-axis of the top accelerometer; Middle diagram: Signal measured by the z-axis of the bottom accelerometer; Lower diagram: ECG signal; All signals were acquired synchronously

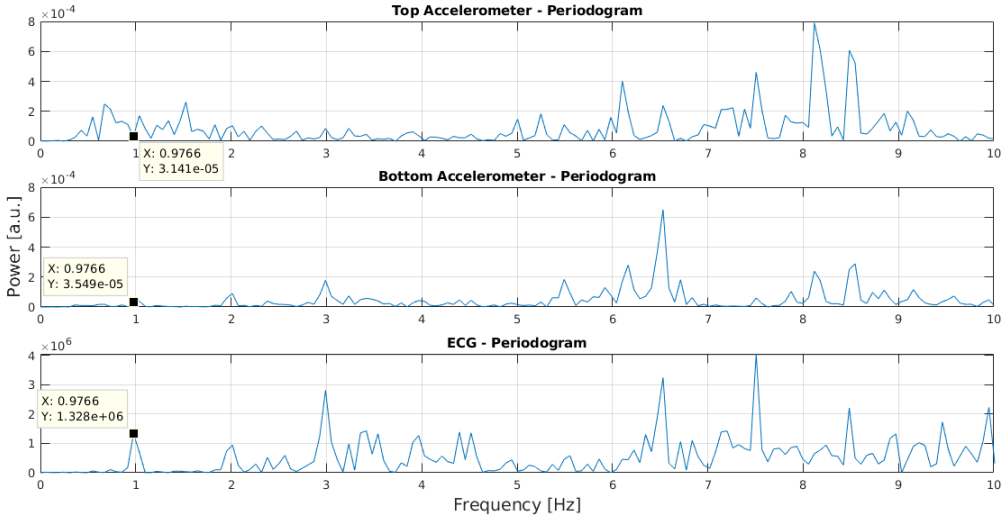

Figure 4.5: Periodogram of the signals presented in Figure 4.4- Upper diagram: Periodogram of the top accelerometer; Middle diagram: Periodogram of the bottom accelerometer; Lower diagram: Periodogram of the ECG signal

It is also observable that *Compression* segments are more stable in the bottom sensor(Figure 4.7), with artifacts contaminating the morphology during these segments in the top accelerometer(Figure 4.6). This contamination is also visible in the periodograms depicted in 4.8. The compression fundamental frequency and its harmonics are not as determined as in Figure 4.9, which concerns the periodograms in the bottom ACC. Hence, the position chosen for the bottom accelerometer provides a higher quality signal.

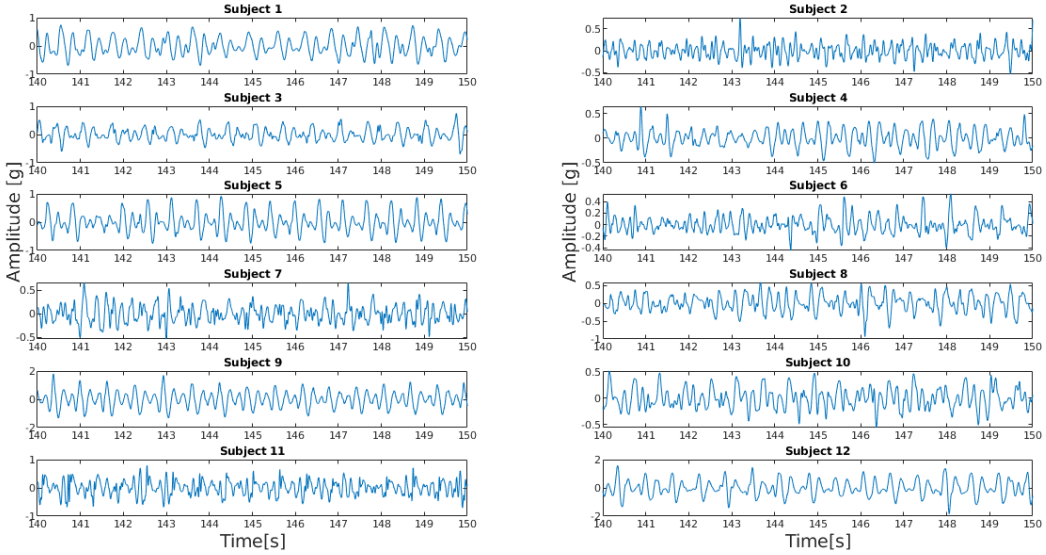

Figure 4.6: 10 seconds of Compressions - Top Accelerometer, z-axis

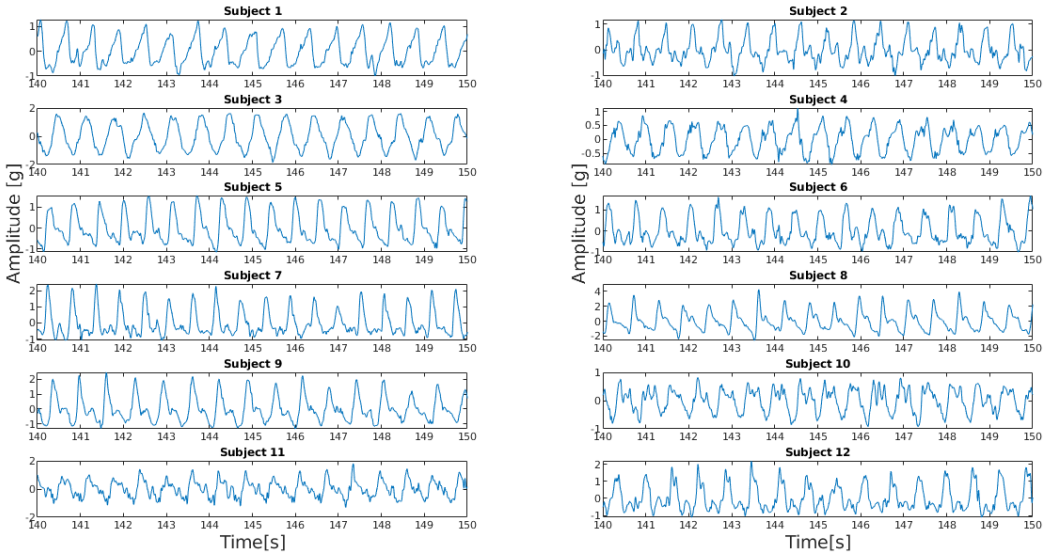

Figure 4.7: 10 seconds of Compressions - Bottom Accelerometer, z-axis

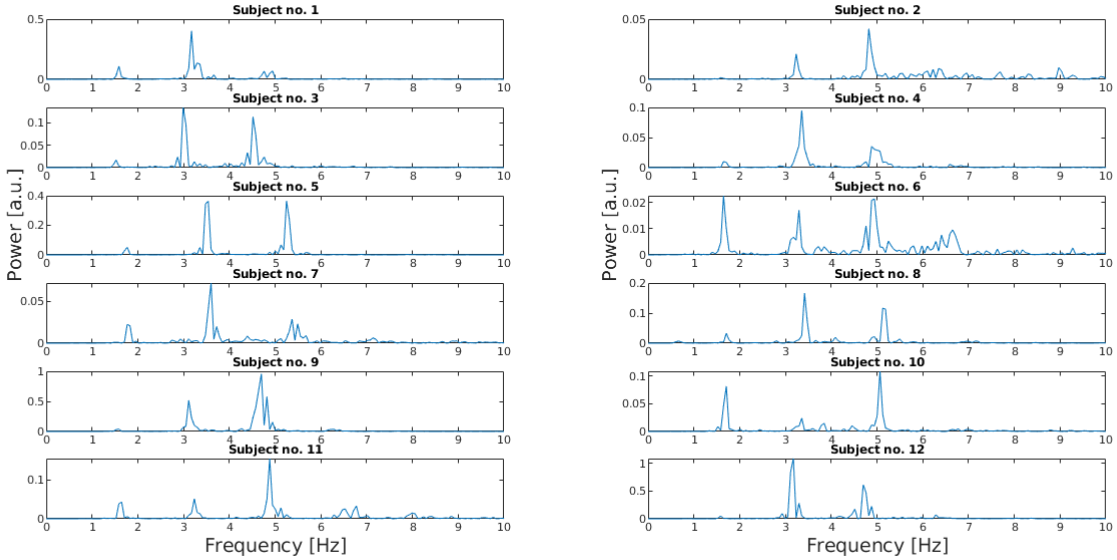

Figure 4.8: Periodogram of the signals from Figure 4.6 - Top Accelerometer

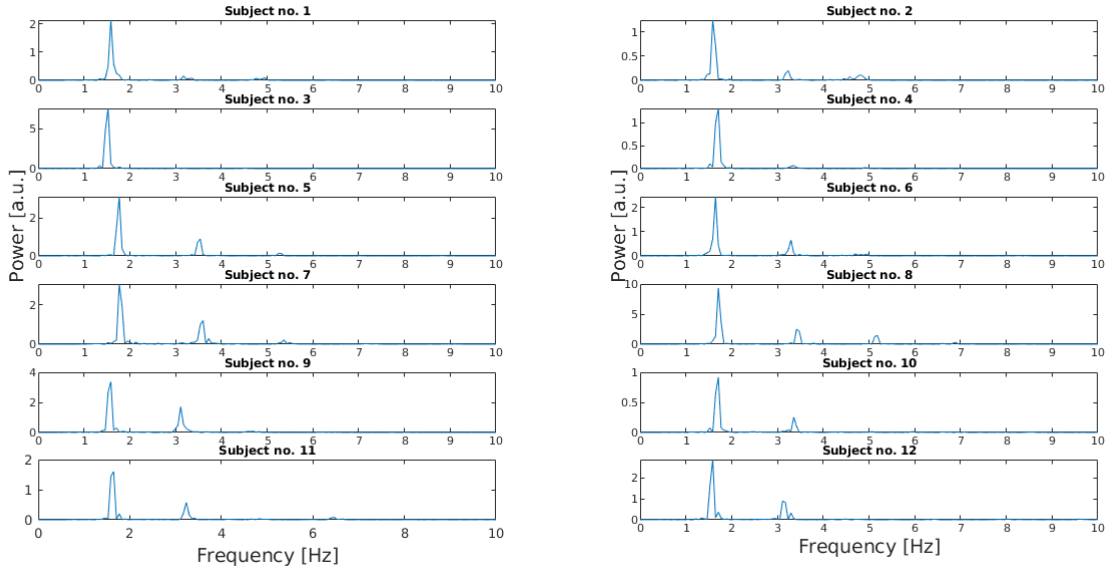

Figure 4.9: Periodogram of the signals from Figure 4.7 - Bottom Accelerometer

Despite a more stable signal being present in the bottom accelerometer, is still important to note that pulse morphology easily changes between subjects(Figure 4.10) and so algorithms developed need to take in consideration this variability and a generalised solution needs to be constructed and tested in a wide dataset to guarantee functionality.

The loss of quality when using a higher position for the accelerometer can be understood when considering that the higher the point of measurement is in the neck,

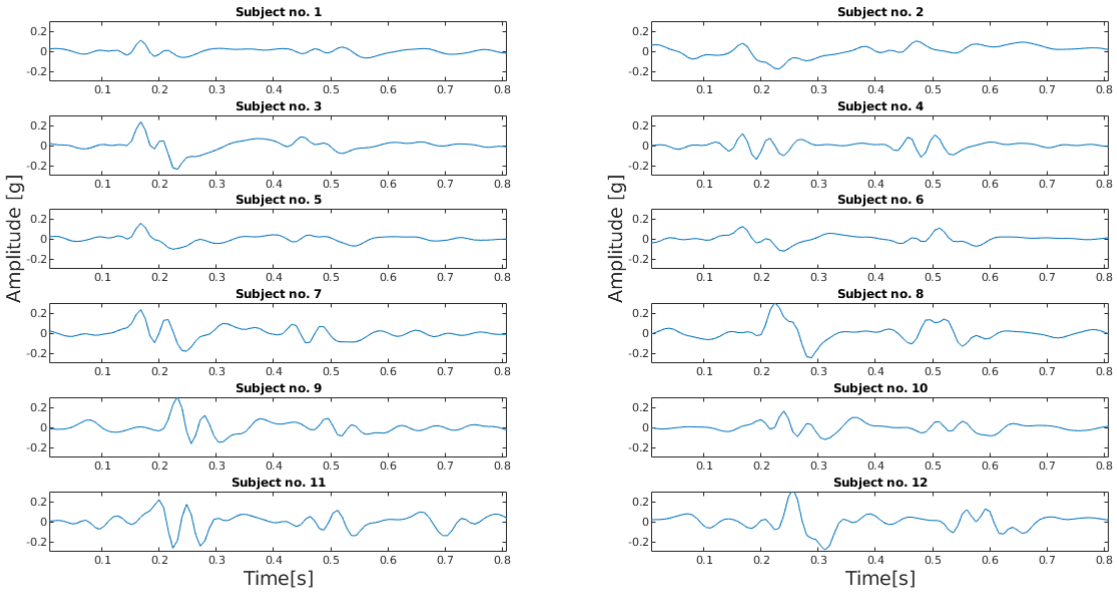

Figure 4.10: Averaged pulse beat morphology for each subject(using 20 manually selected beats) measured by the z-axis of the Bottom Accelerometer

the bigger the dislocation(thus, bigger acceleration) caused by neck movements will be, leading to more noise contamination in the signal measured.

Regarding the capacity of the designed protocol to simulate characteristics visible in real life data it is possible to infer that periodic behaviour was correctly simulated. Looking at Figures 4.8 and 4.7 it is observed that the fundamental frequency is in the expected interval which is suggested by resuscitation guidelines, i.e., [1.66 - 2] Hz. On the other hand morphology behaviour of these segments was not similar to that observed in the real-life data (depicted in Figure 4.11). Higher amplitude, and a more peaky signal is observed in real ACC signals, which can be derived from the CPR procedure directly affecting perfusion to the brain. In spite of this, the correct simulation of periodicity can help in development of feasible technical solutions.

However, some challenges are present in this dataset. One identified challenge in data acquisition regards the body movements and compressions with movements phases. The initial intention for the introduction of these segments was to simulate stochastic artifacts which could appear in a resuscitation scenario. Nevertheless, by making these movements last for 30 seconds the subjects' natural tendency was to induce a certain periodicity in the movements performed. Also adding these movements during compressions does not present a realistic scenario, as depicted in Figure 4.12. Periodic artifacts were present for example during neck movements

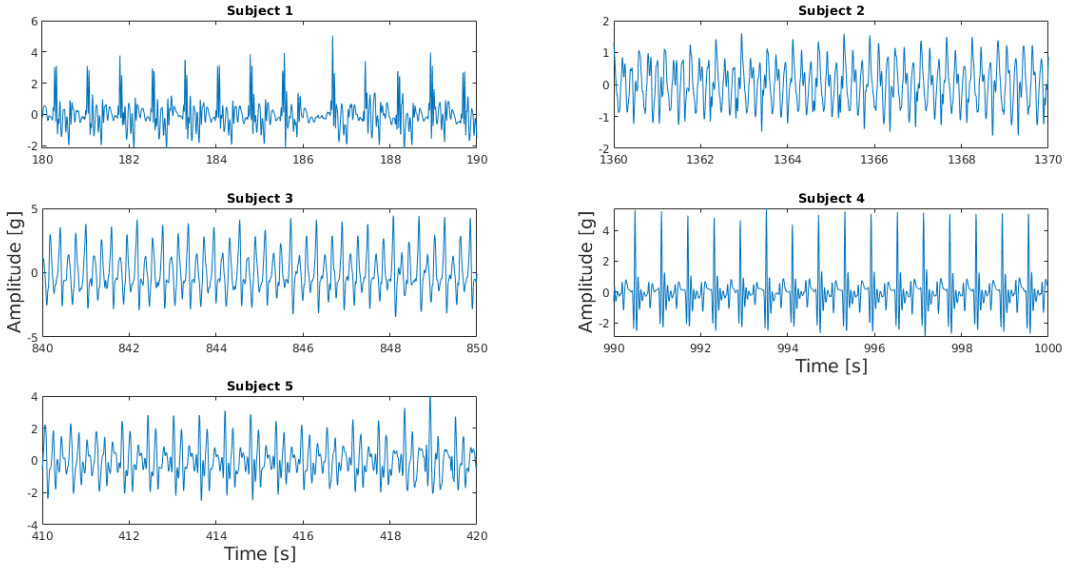

Figure 4.11: 10 seconds of Compressions - Real Life Data, z-axis

phases in the bottom accelerometer which are depicted in Figure 4.13. On the top accelerometer this phases presented a more stochastic behaviour once again showing that different positioning of the sensor lead to very different characteristics(Figure 4.14). However, it is important to emphasise that the replication of movements did not occur in the most realistic manner.

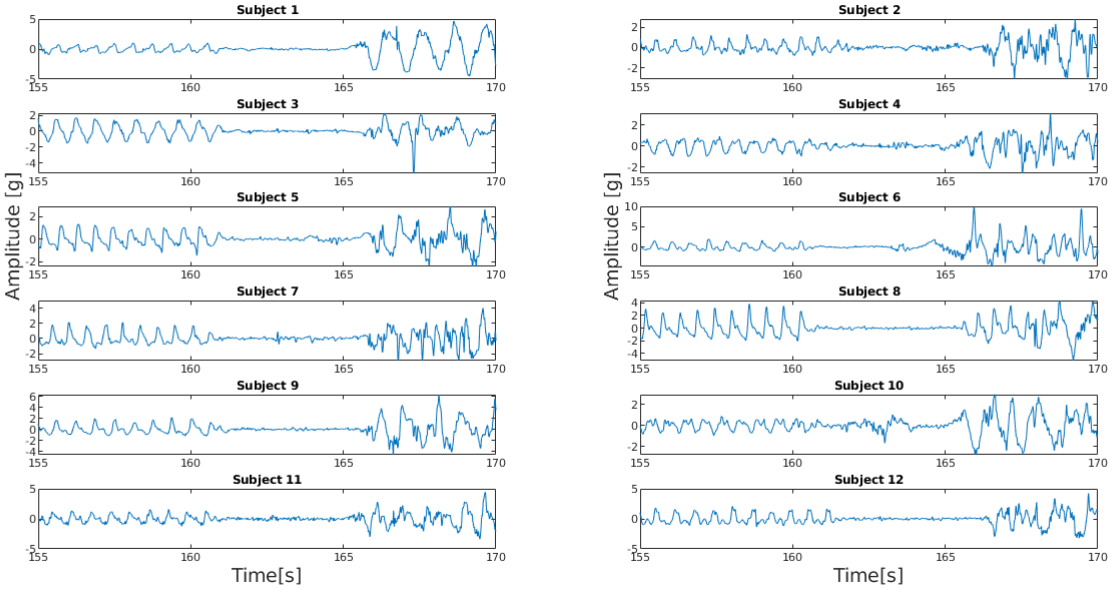

Figure 4.12: Ending of compression phase with beginning of compression with neck movement - Bottom Accelerometer, z-axis

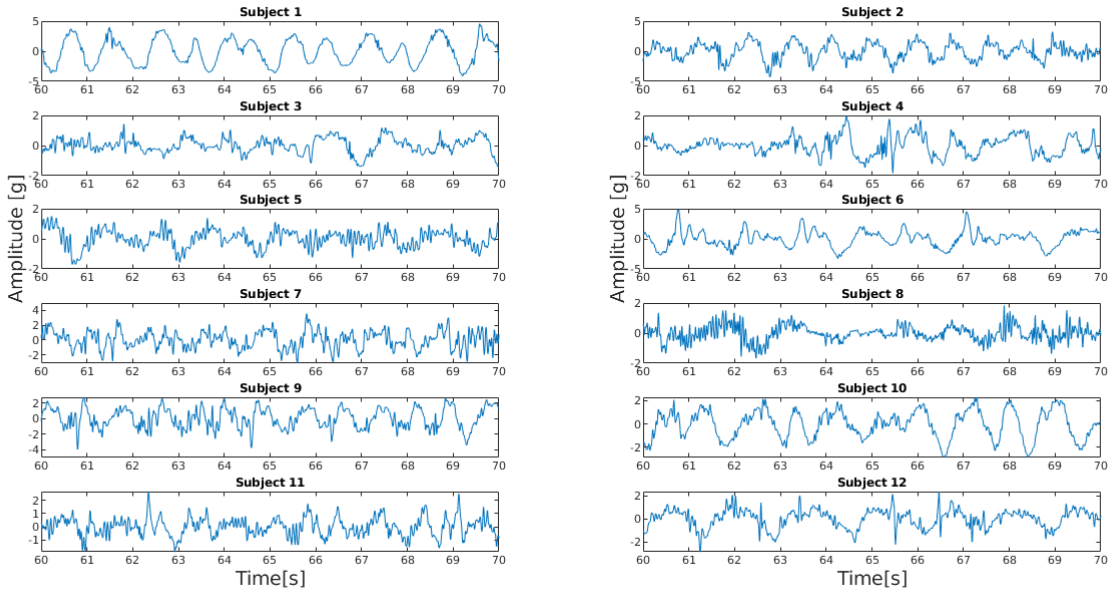

Figure 4.13: Neck movements in simulated data - Bottom accelerometer, z-axis

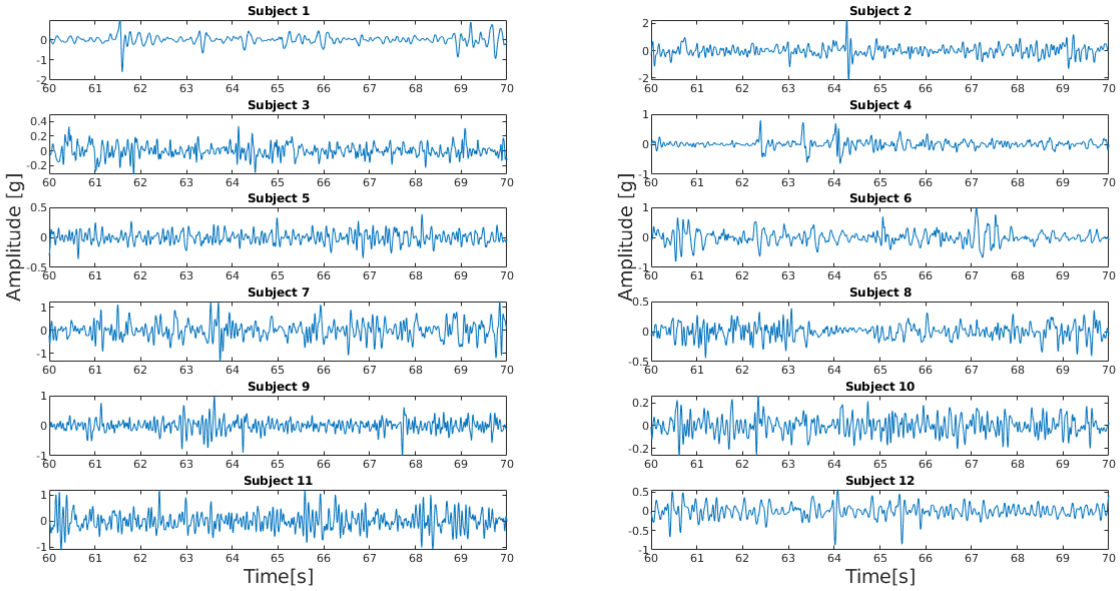

Figure 4.14: Neck movements in simulated data - Top accelerometer, z-axis

4.4 Data Annotation

4.4.1 Protocol Data

For the building of supervised classifiers and for the testing of the performance of the different algorithms implemented, it is necessary to annotate the signal accordingly

with the intended classes. Since the data acquisition was done on healthy subjects, absence of pulse is not present, therefore in the protocol dataset only three distinct labels can be found:

- Pulse
- Compression
- Artifact

Two different annotations were made for the dataset. Initially a sample-by-sample annotation was performed, marking the beginning and ending of each segment containing distinct labels. With this method, future labeling of different window sizes to the one used in the algorithms developed can be easily performed by selecting the mode of the different labels present in the window. However, this method is prone to error. A window contaminated by artifact could still be labeled as pulse if the duration of the artifact was small. Hence, to diminish imprecision and ease the interpretability of the analysis, a second annotation was made where every 3-second window was labeled manually. In this case, windows which corresponded to transitions and therefore had mixed characteristics with ambiguous labeling were also marked so that when training and testing the algorithms implemented only "clean" windows were considered.

It's quite important to remark that labeling without medical expertise is not the most adequate action and undoubtedly it will affect the results obtained and provide a source of error. In this dataset however the main challenges in annotation were related to the distinction between *Compression* and *Artifact* windows. As the protocol includes segments of compressions with added movements and the intensity and periodicity of these movements was varied subject to subject it provided a challenge as some windows were ambiguous. This challenge was mostly observed in the top accelerometer, due to its already mentioned noise contamination and unstable behaviour.

4.4.2 Accelerometer data acquired during real-life cardiopulmonary resuscitation

Similarly to the laboratory acquired dataset it was necessary to annotate the data from real-life CPR scenarios, so as to allow evaluation of the performance of the algorithms developed. In this dataset however, as the data was acquired in five

patients undergoing cardiopulmonary resuscitation in a hospital setting, four distinct labels were present:

- Pulse
- No Pulse
- Compression
- Artifact

Manual annotation was done sample-by-sample. Besides the accelerometer signals, other vital signals were available, such as the arterial blood pressure, one-lead ECG and the capnogram. BP was measured from a catheter inserted in the radial artery. These are particularly helpful for discriminating between *Pulse* and *No Pulse* segments. However, not all patients had the same secondary signals available and in two patients annotation was performed solely based on the ACC signal. As previously mentioned, this dataset is the same as the one used in [1] and the labels established at the time were available. For this study a more restrictive approach was taken with the main difference corresponding to the annotation of artifact segments. In the studies' labels a segment was identified as artifact if it corresponded to a high intensity noise. However, there were segments of the signal where no pulse information was available with lower intensity artifacts present which were not identified(see Figure 4.15). After the sample-by-sample annotation, the label for each window was chosen by the mode of all the samples' labels present in the window. Contrary to the protocol acquired data transitions were not excluded.

It is important to mention that data imbalance was present, as seen in table 4.4.

Table 4.4: Number of windows of each class in the real life data

Patient #	**Number of 3 second windows**			
	Pulse	**No Pulse**	**Compression**	**Artifact**
1	61	90	135	36
2	776	62	82	80
3	372	11	167	20
4	467	21	34	41
5	150	19	177	78

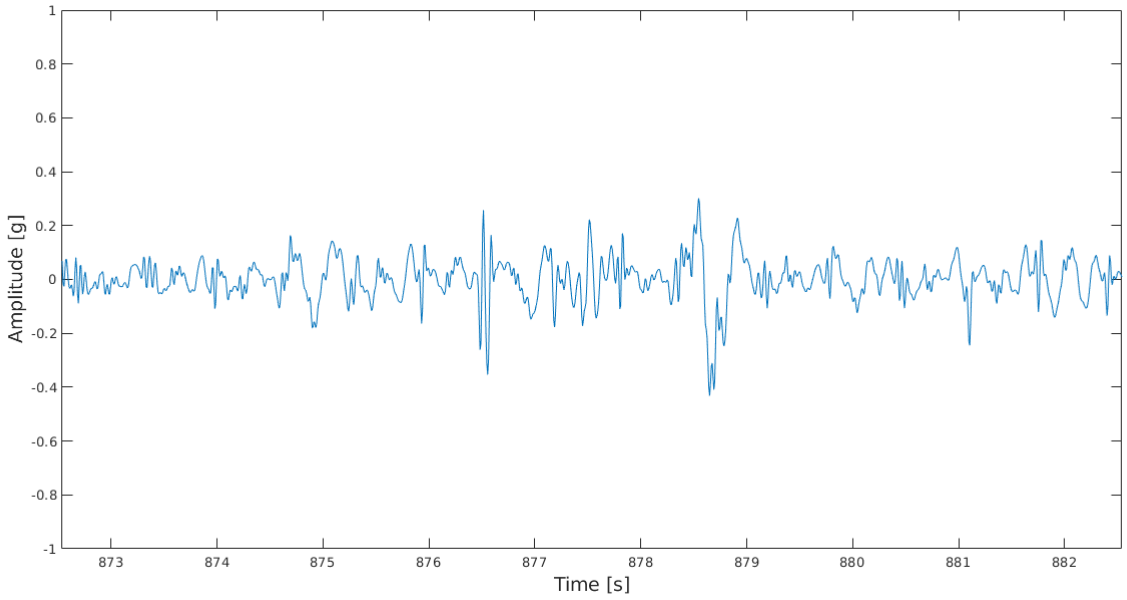

Figure 4.15: Low-intensity artifacts - Real Life Data, z-axis

4.5 Discussion and Future Work

Acquisition of real life data in resuscitation scenarios is complicated. Thus, it's vital to study how to complete real-life datasets by simulated data acquired under controlled conditions, in order to permit further development of technical solutions which can improve care given in resuscitation events. The protocol designed for this study manages to mimic some characteristics adequately and provides a stepping stone for future research by providing a initial database of 12 healthy volunteers, each with synchronous measurements of different vital signals, making it possible to test related hypotheses regarding pulse detection and pulse characterisation. Three possible future works would be:

- Pulse Peak Detection: development of a algorithm for pulse rate extraction, evaluating the results using the heart rate extracted from the ECG
- Pulse Wave Velocity: Feasibility of using two accelerometers positioned along the carotid for calculation of PWV
- Pulse Strength Assessment: Study how pulse signal characteristic correlate with PAT, with the ground truth values calculated from PPG and ECG signal;

From the acquired dataset it is also possible to infer that sensor positioning plays a vital role in signal quality, with the bottom accelerometer presenting a higher quality

signal with less artifact contamination. Pulse frequency is more present in the signals measured by this sensor, and the signal is more well defined, with relatively consistent behaviour between the subjects available. Hence, a more extended study to establish a relatively optimal placement and a guideline which allows for sensor positioning in a quick and effective manner might be of interest. This way, further data collection would present higher quality signals allowing for a better study of the signal's characteristics.

Annotation for both datasets was also performed, providing initial labels for the protocol data and a review on the previously done labels of the real life patients' signals. It is important to emphasise that there were differences in the approach taken for the annotation to the previous study. The main alterations consisted of selection of artifact segments which previously were labeled either as pulse or no pulse segments. These alterations and the fact the labeling did not have medical contribution have to be taken in consideration when analysing the results.

4.6 Conclusion

The data acquisition resulted in a dataset of 12 healthy volunteers which will be used for the development of pulse detection algorithms. It also provides a testing ground for future hypotheses. From the data analysis some conclusions can be drawn. Nevertheless, the dataset needs to be extended for validation and preferably signals from subjects with more varied characteristics should be measured.

The bottom accelerometer presents less artifact contamination and a more consistent morphology, thus it can be expected that results achieved for the signals measured by this sensor will be better. It also demonstrates the morphology's dependency to the sensor position which needs to be taken in consideration during development of techniques.

Success was achieved in simulating some of the characteristics present in real life situations. However the protocol could suffer some alterations for better simulation. One possible alteration would be the reduction of the duration of artifact segments, which would allow for a more stochastic behaviour to be present. Annotation of the data was also provided, though it lacks reviewing. Nevertheless, for analysis of results achieved this fact will be taken in consideration.

5

Pulse Detection using Accelerometer Signals from the neck area with carotid artery underneath

5.1 Introduction

Manual Palpation is still nowadays the most common pulse assessment technique, despite being prone to error and often taking too long compromising patient outcome[13][1]. Thus, there is a clear need of improvement in this intervention. Automatic pulse detection is a solution which could potentially save precious time in resuscitation events and objectify pulse measurement, taking the subjectivity factor from rescuers' palpation. Accelerometers provide a sensing modality with feasibility for pulse detection already proven for healthy subjects via signals from the chest area or at the neck, besides being of easy implementation, cheap and low power, nevertheless presenting high sensitivities[27].

As depicted in Figure 5.1, following preprocessing of the data and extraction of different features, two distinct supervisioned pulse detection algorithms were developed in this work. The first approach consisted in a two-step cascading classifier similar to the one developed by Dellimore *et al.*, which is depicted in Figure 5.2. A first classifier serves to identify a window as *Pulse/No Pulse* or *Compression/Artifact*, with a second and third classifier providing the final classification of each window. This algorithm is built on the assumption that the different classes present distinct characteristics in activity and in periodicity which allows for their sequential separation. However, this method naturally leads to an accumulation of errors seen that a window which is misclassified in the first step will never be correctly classified in

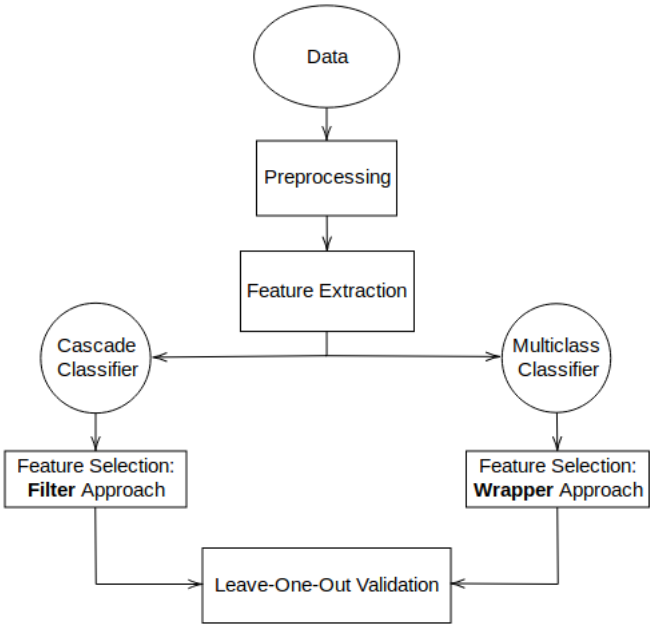

Figure 5.1: Outline of the flow of the algorithm development

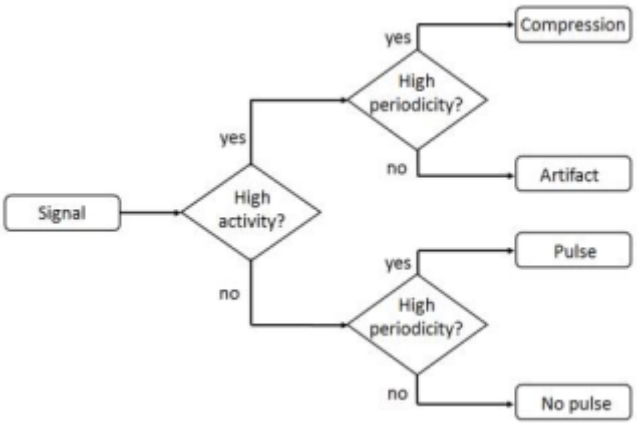

Figure 5.2: Cascade Classifier Logic[1]

the final step. Thus, aiming to diminish this source of error, a second approach was developed consisting of a sole multiclass classifier. For each algorithm, a diferent approach to feature selection was taken. For the cascading classifier a filter approach was used, meaning that feature selection for each step of the final classifier was performed through the use of a feature score parameter. On the other hand, a wrapper approach was chosen for the multiclass classifier, meaning all combinations of features and classifier were tested and using a chosen metric the best combinations were found and presented. For the evaluation of the performance of the algorithms, Leave-One-Out (LOO) validation was performed in the sense that one subject was left out for testing while the remaining were used for training. The procedure was

repeated for all the subjects and the results were averaged, allowing for observation of the behaviour of the solutions developed for each subject and for all of the data.

It is important to mention that besides having a tri-axial accelerometer, calculations were mainly focused on the use of the z-axis, as this axis as been found by previous related studies to be the most significant for the pulse detection problem[30].

5.2 Methods

5.2.1 Feature Engineering

For the development of the classification algorithms it was necessary to extract different features from the accelerometer signal. Preprocessing consisted only of a Butterworth bandpass filter in the range [0.5 30] Hz. The high pass component removed low frequency components such as respiratory movements present, while the high pass component was selected after visual inspection (see Figure 5.3) of the effect of different values in the pulse signals available.

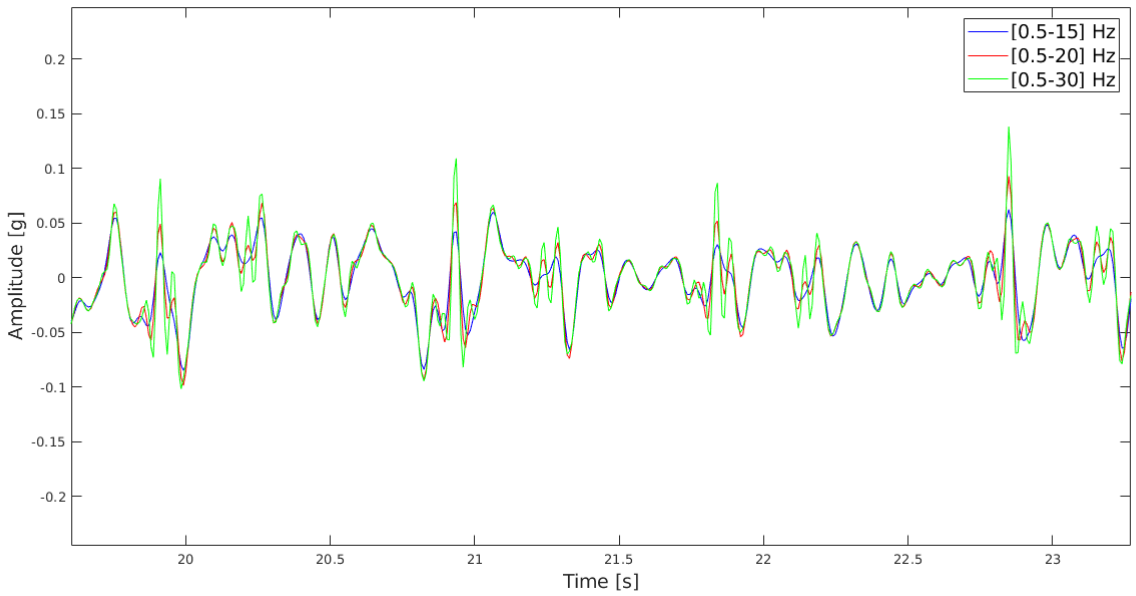

Figure 5.3: Prominence representation(red line in the middle peak)[1]

Feature extraction was performed on non-overlapping 3 seconds windows, with some features being extracted directly in the time domain representation and others from the Phase Space Reconstruction(PSR) of the signal. The latter approach constitutes

a non-linear dynamic signal processing technique and has provided good results on ECG characterisation[46] and Heart Sound Classification[47]. Its applications in accelerometry has also achieved effectiveness when applied to activity and gait recognition[48]. However, its use for accelerometer based pulse detection is a novel contribution.

Feature engineering is usually defined as the process of extracting information from the data source which is able to adequately compress the domain. There are at least the following approaches for feature engineering:

- Extraction of features based on domain knowledge: this process is usually applied in contexts where the processes involved in the signal generation are reasonably known and it is possible to define specific features to capture relevant characteristics of the signal.
- Extraction of features not based on domain knowledge: in this approach the aim is to capture fundamental information which might prove useful, using different feature extraction techniques. Afterwards, feature reduction techniques(such as a feature selection score) are usually applied to simplify the feature sphere.
- Feature learning: In this situation a data-domain approach is followed to automatically identify relevant features using techniques such as auto-encoders or deep learning.

In this work, the first two approaches were used, as commonly techniques related to feature learning require large amounts of data to effectively represent the data. Identified relevant domain knowledge in the context of this thesis are activity level and periodicity. *Pulse* and *No Pulse* are usually low amplitude signals, whilst *Artifacts* and *Compression* are commonly higher amplitude signals. *Pulse* and *Compression* segments are also usually characterised by their periodicity, with the latter presenting common values of periodicity in the interval [60 100] beats per minute and the former in the interval [100 120] compressions per minute. With the introduction of each feature a brief explanation on the reasoning behind its extraction will be presented.

5.2.1.1 Time Domain Representation

Ten features were extracted from the time domain representation:

- Standard Deviation(STD) - Mean of the standard deviation of every sample

in the window. The mean of the signal is not subtracted in the formula for it is assumed that it equals zero, as the signal is filtered in the range [0.5 30] Hz. With this feature activity of the window is measured.

$$STD[wdw] = \sqrt{\frac{1}{N_{wdw}} \sum_{k=n-N_{wdw}+1}^{n} acc_z^2[k]} \tag{5.1}$$

- Teager Energy(TE) - Mean of the teager energy operator value for all the samples in the window. This feature both presents a measure of amplitude as well as introducing a frequency component as the calculated value for each sample uses both the previous and next sample amplitude. It is a very interesting feature in this context as both compressions and pulse have a well defined

$$TE[wdw] = \frac{1}{N_{wdw}-1} \sum_{k=n-N_{wdw}+2}^{n-1} (acc_z^2[k] - acc_z[k-1]acc_z[k+1]) \tag{5.2}$$

- Prominence(PM) - measured by extracting the peak prominence of the highest peak in the autocorrelation of the signal in the window. The prominence of a peak is calculated by creating two lines to each side of the peak until said lines again cross the signal, establishing two intervals. Afterwards the minimum of each interval is found and the maximum of the two values is established as the reference. The difference between the peak's height and the reference corresponds to the prominence(see Figure 5.4).

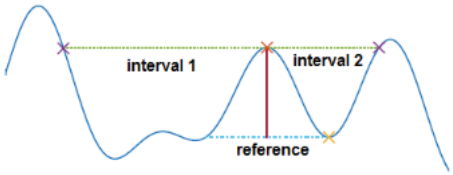

Figure 5.4: Prominence representation(red line in the middle peak)[1]

The autocorrelation function of the signal presents a measure of similarity of the signal with a delayed version of itself in function of the time delay. When used on periodic signals it is an important tool for assessing periodicity, as it will itself present a periodic behaviour with a higher correlation measured at the time delays associated with the period. By measuring the prominence of the highest peak, we are measuring how relevant this peak is compared to other neighouboring peaks in the function.

- Module of the lag of the highest peak in the autocorrelation of the window signal(LHP) - By measuring the time delay which corresponds to the highest value of the autocorrelation function, the aim is to calculate the inverse of the estimated fundamental frequency of the window. This assumption is based on the expected autocorrelation from a periodic signal. As seen in Figure 5.5, despite the fact that this feature does not present a discriminative behaviour for all the classes in *Pulse* and *Compression* windows the value is relatively stable, leading to the inference of its utility for rate characterisation.

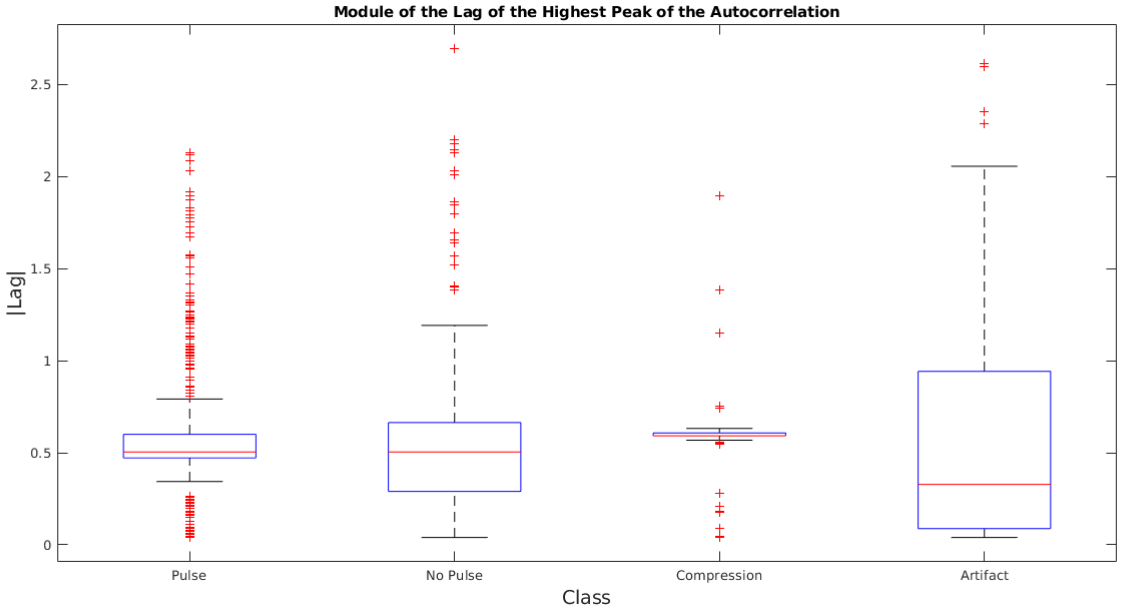

Figure 5.5: Boxplot of the LHP calculated in all the real-data patients

- Average Power of the 4 highest peaks of the window signal's periodogram(P_{4Peaks}) - The periodogram presents an estimate of the power spectral density of the signal. Thus, it allows for a frequency analysis of the signal, with frequencies most present in the signal having more power. In a periodic signal the fundamental frequency and its harmonics will present a higher power than other frequencies. Hence, by averaging the power of the four highest peak of the periodogram of each window a frequency characterisation is being performed.
- Standard Deviation of the cross-correlation($\tau_{delay} = 0$) between the ACC's x and z axis(STD_{xz}) - Despite the z-axis being the most relevant for pulse detection, other axis also present relevant information(see Figure 5.6). The reasoning behind the extraction of this feature was that in periodic movements the correlation between axis will present less dispersion compared to when stochastic noise is present, as periodic components will be present in all axis

with similar behaviour.

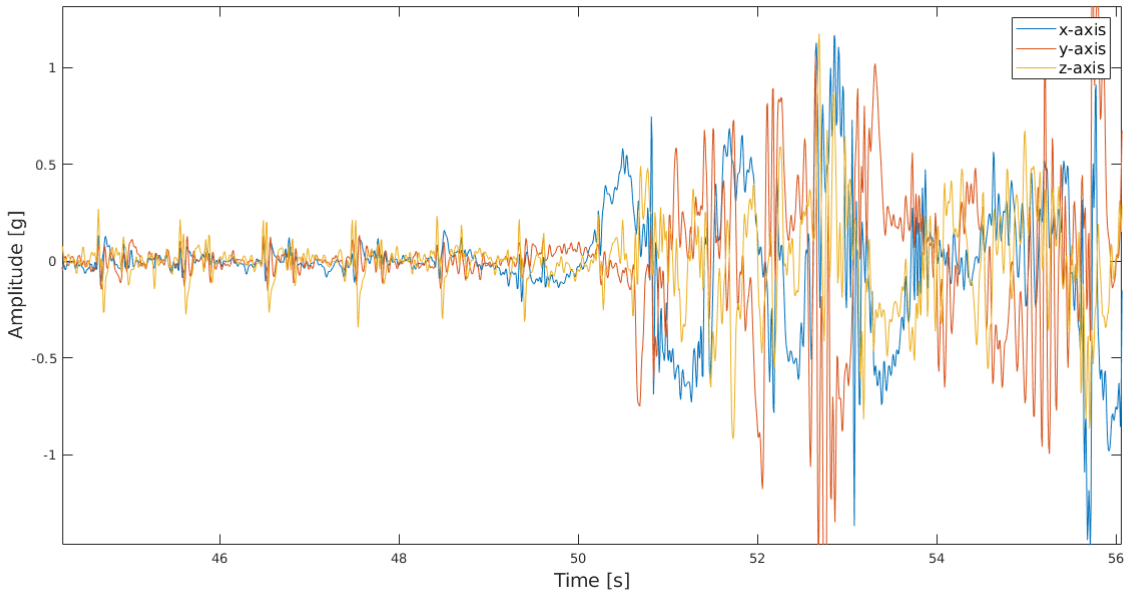

Figure 5.6: Pulse and Artifact Segment - Changes in the correlation over the different axis

$$CCF_{\tau_{delay}=0} = acc_x[wdw] * acc_z[wdw] \tag{5.3}$$

$$STD_{xz}[wdw] = \sqrt{\frac{1}{N_{wdw}} \sum_{k=n-N_{wdw}+1}^{n} (CCF_{\tau_{delay}=0}[k] - \overline{CCF}_{\tau_{delay}=0})^2} \tag{5.4}$$

- Standard Deviation of the cross correlation($\tau_{delay} = 0$) between the ACC's y and z axis(STD_{yz}) - calculated identically to STD_{xz}
- Standard Deviation of the ACC signal derivative($\text{STD}_{acc'}$) - A measure of the stability of the dispersion of the derivative signal. Uncontaminated segments will present a more stable behaviour

$$STD_{acc'}[wdw] = \sqrt{\frac{1}{N_{wdw}} \sum_{k=n-N_{wdw}+1}^{n} (acc'_z[k] - \overline{acc'_z[wdw]})^2} \tag{5.5}$$

- Skewness(SK) - Studying the third standardised moment allows for the analysis of the assimetry of the probability distribution of the samples in the window

$$SK[wdn] = \frac{\frac{1}{N_{wdn}} \sum_{k=n-N_{wdw}+1}^{n} (acc_z[k] - \overline{acc_z[wdn]})^3}{(\sqrt{\frac{1}{N_{wdn}} \sum_{k=n-N_{wdw}+1}^{n} (acc_z[k] - \overline{acc_z[wdn]})^2})^3} \tag{5.6}$$

- Kurtosis(KU) - The fourth standardised moment, as the third also allows for the analysis of a property of the probability distribution of the values. However, in this case it presents a measure of the shape of the tails of the distribution.

$$KU[wdn] = \frac{\frac{1}{N_{wdn}} \sum_{k=n-N_{wdw}+1}^{n} (acc_z[k] - \overline{acc_z[wdn]})^4}{(\sqrt{\frac{1}{N_{wdn}} \sum_{k=n-N_{wdw}+1}^{n} (acc_z[k] - \overline{acc_z[wdn]})^2})^2} \tag{5.7}$$

5.2.1.2 Phase Space Reconstruction

PSR is a technique used for the representation of the non-linear characteristics of a dynamic system[49]. It can be achieved by two different methods, delay coordinates or derivative coordinates[47]. In this work the former method was adopted with a N-point time series $\{x_1, x_2, ..., x_N\}$ being reconstructed into each phase-space vector $\mathbf{X}_i$ as follows:

$$X_i = [x_i, x_{i+\tau}, x_{i+2\tau}, ..., x_{i+(m-1)\tau}] \tag{5.8}$$

In 5.8 τ corresponds to the reconstruction delay and m to the embedding dimension. The embedded matrix will then correspond to a $M \times m$ matrix, where $M = N - (m-1)\tau$.

For successful extraction of features of the PSR it is necessary to choose the parameters of its composition accordingly, with the delay parameter being chosen before the dimension. An optimal τ should be computed so as to not have a value which is neither too small, being equivalent to a large correlation between x_i and $x_{i+\tau}$, or too big, resulting in the two vectors being completely independent. The optimisation of this value can then be performed using the mutual information between x_i and $x_{i+\tau}$

$$I(\tau) = \sum_{n=1}^{N-\tau} p(x_i, x_{i+\tau}) log_2 \frac{p(x_i, x_{i+\tau})}{p(x_i)p(x_{i+\tau})} \tag{5.9}$$

where $I(\tau)$ is the mutual information, and p the probability. The value chosen corresponds to the first minimum that occurs in mutual information. Since the data presents different dynamics the optimal value was calculated for each window and

in the end the average was calculated, with the value of $\tau = 4$ being found for both the Top and Bottom accelerometer data.

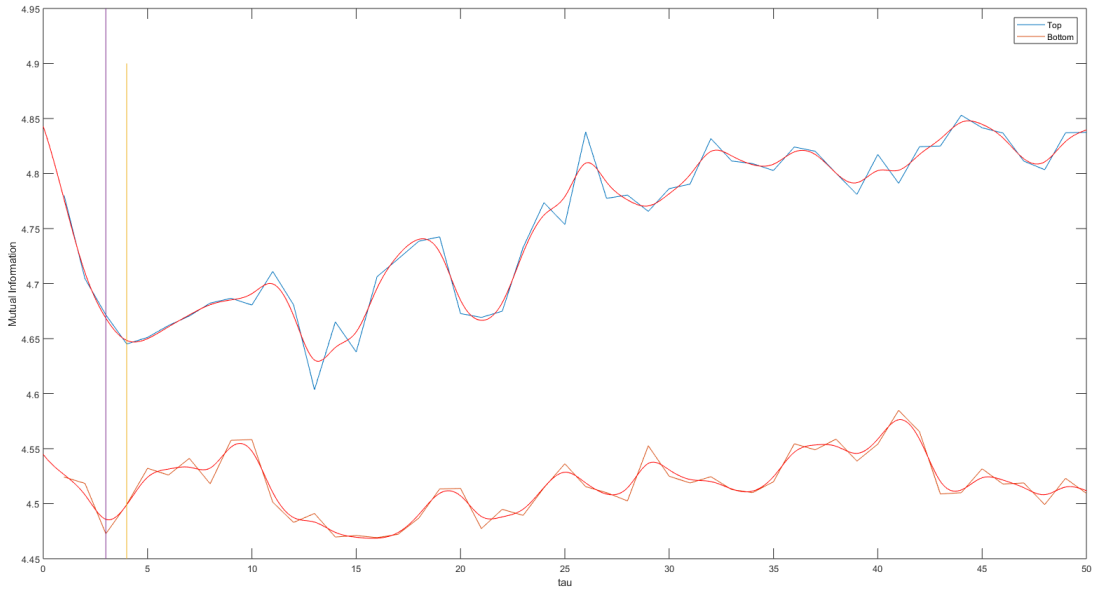

Figure 5.7: Reconstruction delay parameter calculation for one 3 second window of Top(blue) and Bottom(red) accelerometer data

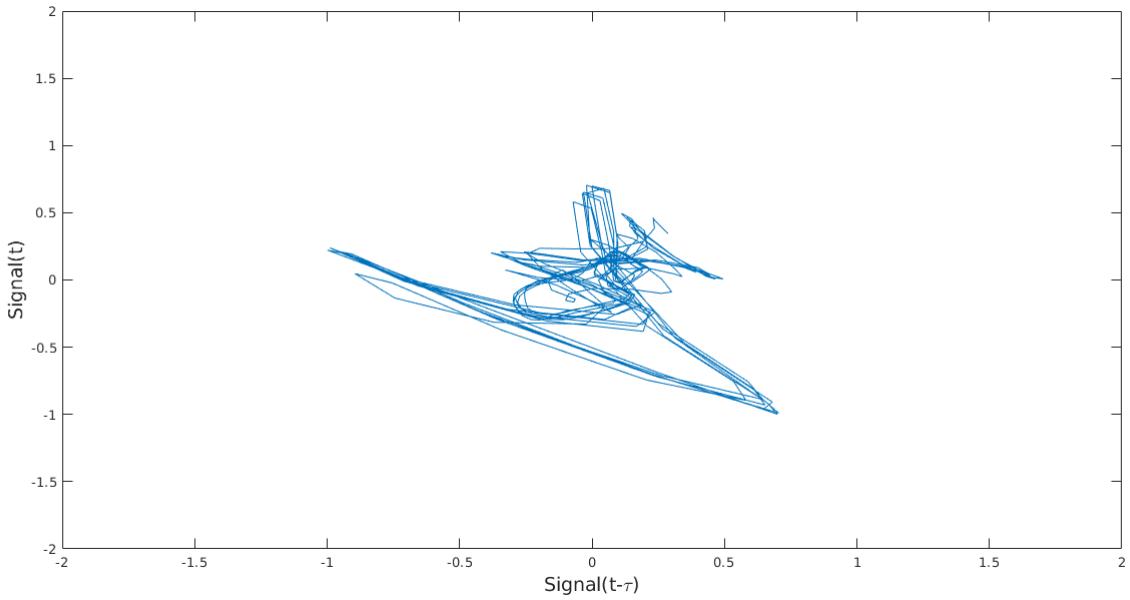

Figure 5.8: Example of a bi-dimensional PSR

Corcerning the embedding dimension, a value of $m = 2$ was chosen initially, in order to simplify the interpretation of the phase space in a graphical aspect(see Figure

5.8). However, for one feature it was decided that optimisation of this parameter was necessary. The method used was the well known Cao's method[50]. According to this method if a value of m is the true embedding dimension of the reconstructed vector, the two points which are closer in the m dimensional phase space will remain closer in the $m+1$ dimensional phase. Cao's method embedding function is defined as

$$E(m) = \frac{1}{N - m\tau} \sum_{i=1}^{N-m\tau} a_i(m) \tag{5.10}$$

with $a_i(m)$ defined as follows

$$a_i(m) = \frac{||Y_i(m+1) - Y_{n(i,m)}(m+1)||}{||Y_i(m) - Y_{n(i,m)}||} \tag{5.11}$$

where $Y_{n(m,i)}$ represents the nearest neighbour of $Y_i(m)$ in the m-dimensional space. Computation of the nearest neighbour is based on a measure of distance which uses the maximum norm function. In order to model the variation from m to $m+1$ it is necessary to define another function

$$E_1(m) = \frac{E(m+1)}{E(m)} \tag{5.12}$$

which converges to 1 in case of a finite dimensional attractor. However, as this may occur even with random signals it is necessary to define another function which allows to distinguish between deterministic and random data. This function is defined as follows

$$E_2(m) = E^*(m+1)E*(m) \tag{5.13}$$

with

$$E^* = \frac{1}{N - m\tau} \sum_{i=1}^{N-m\tau} |x_{i+m\tau} - x_{n(i,m)+m\tau}| \tag{5.14}$$

In case of a random signal a constant value of one will be present in $E_2(m)$ for all different values of m. If at least for one value of m the value is different from one the signal is found to be deterministic. The embedding dimension for PSR is set to a minimum embedding dimension. Once again, as different dynamics were present in the signal the optimal m was calculated for each window and averaged for computation of the final value of $m = 4$ for both datasets of the protocol data. Depicted in Figure 5.9 is an example of the computation of the embedding dimension.

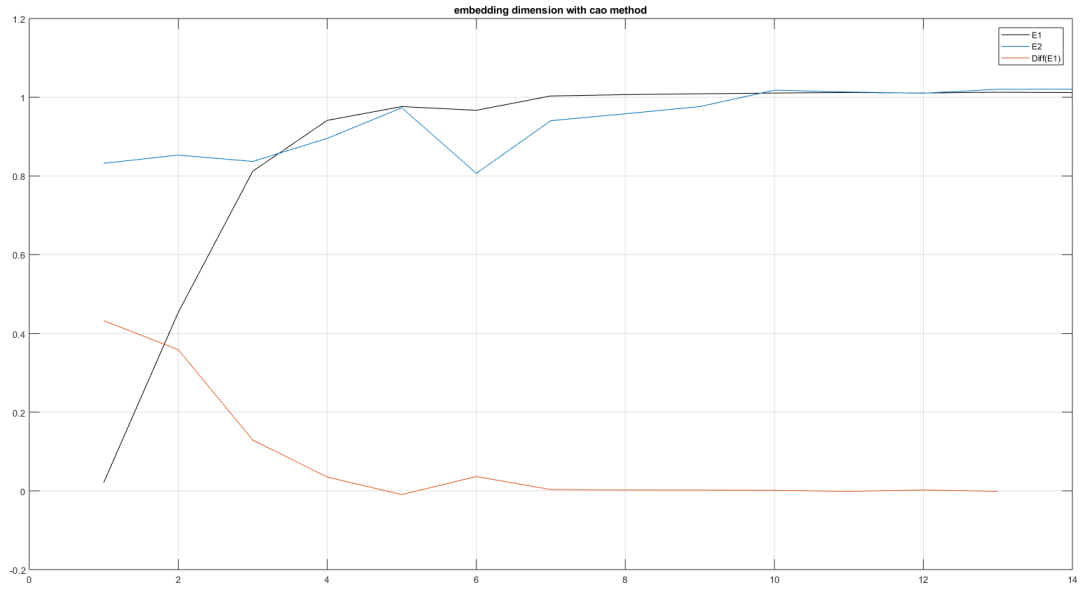

Figure 5.9: Reconstruction embedding dimension parameter calculation for one 3 second window of Top and Bottom accelerometer data

Having the reconstructed phase space parameters determined it is then possible to extract different features from each PSR of a window. It is important to mention that the signal was not normalised as very different amplitudes limited the feature extraction, and for this work manually defined limits were set for the phase space. If points were of bigger amplitude than that of the limit they were not considered for the calculations of the features. The limits were set, after visual inspection of the data, so that outliers in the signals were removed, as follows

$$limit_{top/bottom} = \overline{acc}_{ztotal} \pm 5 * \sigma_{total} \tag{5.15}$$

$$limit_{real} = \overline{acc}_{ztotal} \pm 8 * \sigma_{total} \tag{5.16}$$

with acc_{ztotal} corresponding to the concatenated vector of all different subjects' z-axis signals of each sensor. In 5.10 and Figure 5.11 a visualisation of the concatenated filtered signals and limits is depicted.

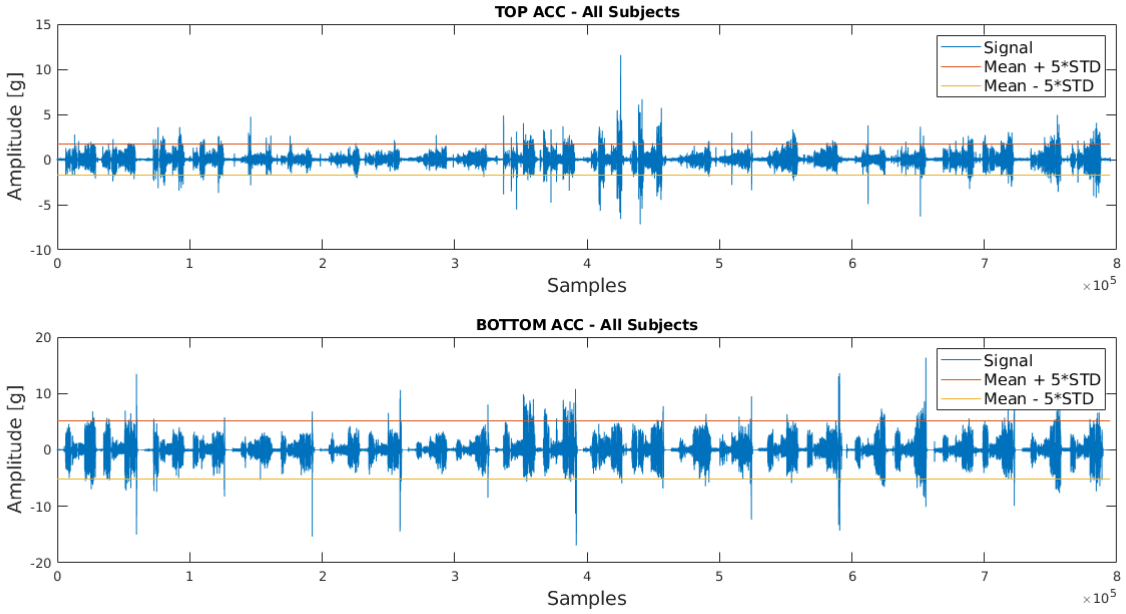

Figure 5.10: Concatenated signals from all subject of the simulated data with PSR limits shown. Upper Diagram: Top ACC; Lower Diagram: Bottom ACC

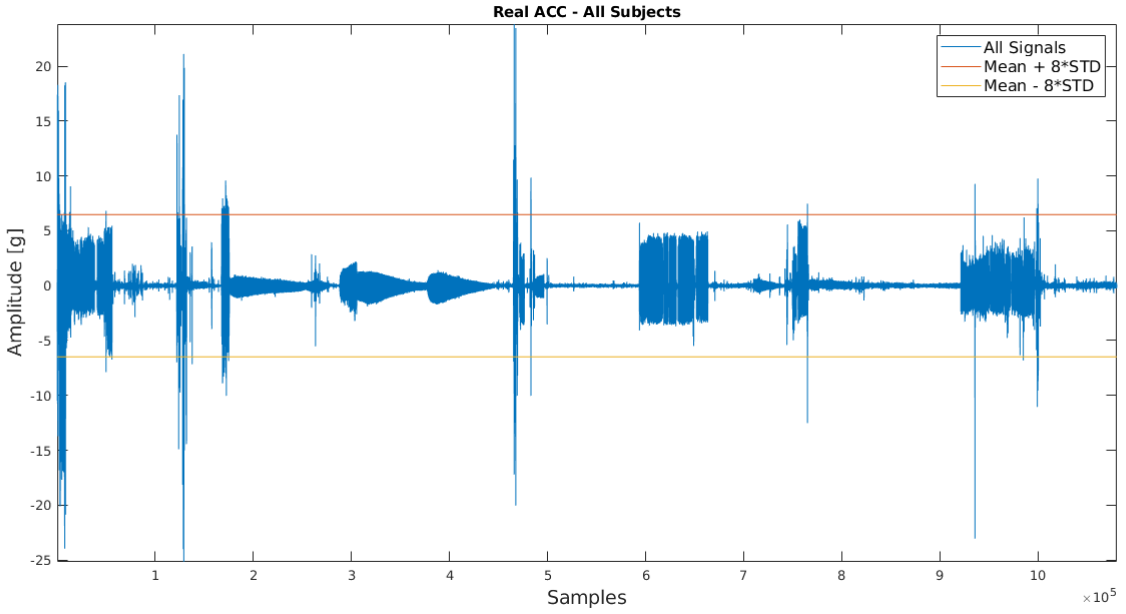

Figure 5.11: Concatenated signals from all subject of the real-life data with PSR limits shown

The features extracted, which aimed to study the distribution of points in the PSR and their closeness, were then:

- Spatial Filling(SF) - Consider the two-dimensional PSR of the accelerometer

signal $x(1)$,$x(2)$,...,$x(n)$. The A matrix is obtained as

$$A = \begin{bmatrix} x(1) & x(1+\tau) \\ x(2) & x(2+\tau) \\ \vdots & \vdots \\ x(n-\tau) & x(n) \end{bmatrix} \tag{5.17}$$

By dividing this phase space into a grid $g(i,j)$ of small squares, a phase space matrix C can be generated in which each element $C(i,j)$ is equal to the number of phase space points falling into the grid $g(i,j)$. Afterwards, a new matrix P can be obtained by dividing each element of C by the sum of all the points present in the initial phase space:

$$P = \frac{1}{M}C, \quad M = \sum_{i,j=1}^{N} C(i,j) \tag{5.18}$$

Hence, the P matrix represents the probability of a space point falling into a certain element of the grid. By squaring this matrix, the R matrix is determined. Considering S as the sum of all points of R, the spatial filling index can finally be computed as

$$SF = \frac{S}{N^2} \tag{5.19}$$

- Area of the C-column average Curve($\mathrm{AUC}_{C-curve}$) - By calculating the average of each column of the C matrix, a curve which characterises the distribution of the points in the phase space is obtained and the relative area of the right extremity was used as feature. This extremity was selected by analysing the mean of all the curves for each class, depicted in Figure 5.12.

- Entropy(EN) - Calculated using the P matrix previously mentioned, as follows

$$EN = \sum_{i,j=1}^{N_{squares}} P(i,j) log_2(\frac{1}{P(i,j)}) \tag{5.20}$$

- Simplicity(SM) - all the previously features were calculated using the bi-dimensional phase space, however for the calculation of the simplicity the embedding dimension was four as calculated by the Cao's method. Hence, having the 4-D phase space $\mathbf{X}_{4D}$ the feature is calculated based on the entropy of the normalised eigenvalues of $\mathbf{X}_{4D}$. For this end, the covariance matrix is

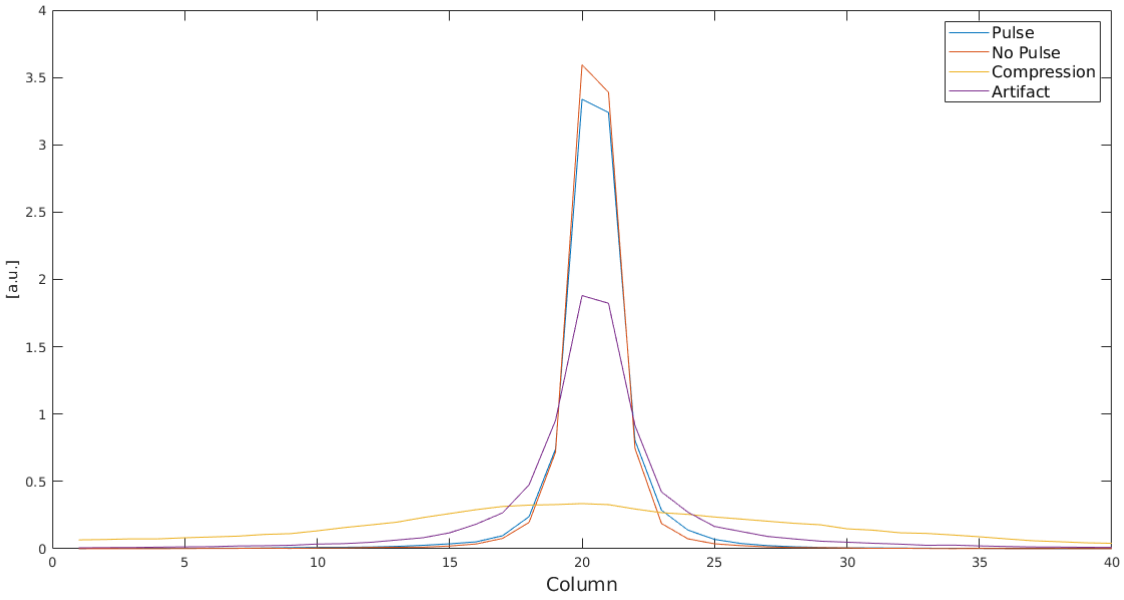

Figure 5.12: Average of the C-Column average Curve for each class

initially obtained by

$$Cov = X_{4D}^{T} X_{4D} \tag{5.21}$$

where T denotes the transpose of the matrix. Let λ_1,λ_2,...,λ_m be the eigenvalues of the covariance matrix and $\hat{\lambda}_1$,$\hat{\lambda}_2$,...,$\hat{\lambda}_m$ the normalised eigenvalues,the entropy of the normalised eigenvalues, H, is calculated by

$$H = -\sum_{i=1}^{m} \hat{\lambda}_i log_2 \hat{\lambda}_i, \qquad \hat{\lambda}_i = \frac{\lambda_i}{\sum_{k=1}^{m} \lambda_k} \tag{5.22}$$

Finally, simplicity is calculated from the entropy

$$SM = \frac{1}{2^H} \tag{5.23}$$

5.2.2 Classifiers for Pulse Detection using accelerometers in the neck area

5.2.2.1 Cascading Classifier

The first algorithm developed in this work, was an extension on previous work by Dellimore *el al.*[1]. It was on this previous study that the real-life dataset was col-

lected and studied for the first time, with the researchers performing a first analysis on the use of a accelerometer sensor in the carotid for pulse detection solutions during cardiopulmonary resuscitation. In said analysis only two simple features were used, specifically Standard Deviation and Prominence(also used in this work). As depicted in 5.2 the classifier logic was built on the assumption of higher activity levels of *Compression* and *Artifact* windows and the lack of periodicity in *No Pulse* and *Artifact* segments. Hence, the two features selected, with STD providing a measure of activity and PM a measure of periodicity. Relevant results were achieved with activity classification performing with high sensitivity and specificity and compression periodicity also showing acceptable results. However, pulse periodicity classification lacked consistency. It's important to mention that the study performed a subject-dependent analysis with thresholds for both features being defined optimally. Thus, maintaining the classifier logic, interest was found in introducing more features as well as training and testing automatic classifiers using a LOO validation, i.e., performing a subject-independent analysis.

The algorithm developed was trained and tested in the two existent datasets, with the limitation that in the laboratory acquired data there was no data without pulse. Thus, in the two sensors of this dataset the cascade classifier logic only comprised two classifiers as depicted in Figure 5.13.

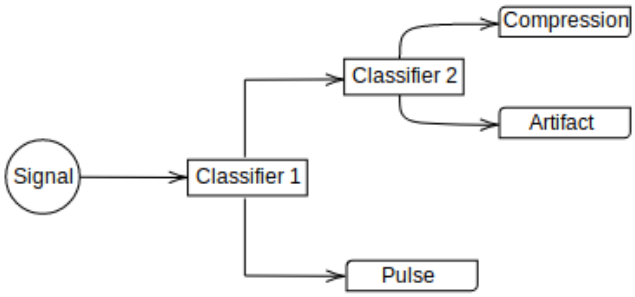

Figure 5.13: Cascade Classifier Logic on the protocol data

Feature selection for each classifier in the algorithm was executed by a filter approach, using a Feature Selection Score(FSS) which combines relevance measured by the area under the receiver operating characteristic (ROC) curve (AUC) and redundancy computed by Spearman's rank correlation coefficient(RCC)[22]. Initially

only the feature with the highest AUC is present in the subset with subsequent features being added according to the highest FSS in each iteration[51]. The formula for the score is as follows

$$FSS_i = AUC(f_i) - \frac{|\sum_{f_j \in S} RCC(f_i, f_j)|}{|S|} \tag{5.24}$$

with $AUC(f_i)$ representing the AUC of the ith feature, $RCC(f_i,f_j)$ the Spearman's RCC between two features, S the subset of features at each iteration and $|S|$ its cardinality.

The FSS scores for each sensor and dataset can be found in Tables 5.1, 5.2 and 5.3, with the features selected for each classifier represented in bold.

Table 5.1: FSS for each classifier - Top Accelerometer

Pulse VS (Compression & Artifact)			Compression VS Artifact		
Feature	FSS	AUC	Feature	FSS	AUC
STD$_{xz}$	0.9962	0.9962	**Simplicity**	0.8455	0.8455
Skewness	0.5659	0.6152	**Teager Energy**	0.6032	0.6947
STD$_{acc'}$	0.6085	0.9851	Kurtosis	0.5721	0.7499
Kurtosis	0.5356	0.7108	Prominence	0.7152	0.7943
Simplicity	0.7006	0.8330	Skewness	0.5527	0.6557
Spatial Filling	0.6210	0.9931	STD$_{acc'}$	0.5213	0.7042
Entropy	0.8445	0.9944	LHP	0.4447	0.4942
Teager Energy	0.7218	0.9865	Entropy	0.2661	0.5642
P$_{4Peaks}$	0.6236	0.9932	AUC$_{C-curve}$	0.1946	0.6041
STD$_{yz}$	0.5571	0.9918	STD	0.0968	0.5605
LHP	0.5263	0.5747	STD$_{xz}$	0.047	0.5098
STD	0.5522	0.9943	STD$_{yz}$	-0.0506	0.4812
Prominence	0.4721	0.5762	Spatial Filling	-0.1258	0.4198
AUC$_{C-curve}$	0.3226	0.7886	P$_{4Peaks}$	-0.0156	0.4460

Table 5.2: FSS for each Classifier - Bottom Accelerometer

Pulse VS (Compression & Artifact)			Compression VS Artifact		
Feature	FSS	AUC	Feature	FSS	AUC
STD	0.9991	0.9991	**Prominence**	0.8920	0.8920
Skewness	0.4441	0.5044	**STD**$_{xz}$	0.7837	0.8024
Kurtosis	0.642	0.9378	Skewness	0.7738	0.8185
Simplicity	0.9293	0.9361	LHP	0.7824	0.8154
STD$_{acc'}$	0.767	0.9891	STD$_{acc'}$	0.6282	0.8562
Teager Energy	0.6115	0.9917	Kurtosis	0.5634	0.6866
Prominence	0.5321	0.5572	Teager Energy	0.5206	0.8443
STD$_{yz}$	0.5731	0.9987	Simplicity	0.4268	0.5308
Spatial Filling	0.5043	0.9985	STD$_{yz}$	0.3798	0.7870
Entropy	0.6663	0.9991	Spatial Filling	0.3182	0.7829
STD$_{xz}$	0.6009	0.9976	Entropy	0.4552	0.7801
P$_{4Peaks}$	0.5499	0.9985	AUC$_{C-curve}$	0.3521	0.7493
LHP	0.4678	0.6368	STD	0.2741	0.7057
AUC$_{C-curve}$	0.2624	0.7553	P$_{4Peaks}$	0.1996	0.6594

Table 5.3: FSS for each classifier - Real Life Data

(Pulse & No Pulse) VS (Compression & Artifact)			Compression VS Artifact			Pulse vs No Pulse		
Feature	FSS	AUC	Feature	FSS	AUC	Feature	FSS	AUC
STD$_{yz}$	0.9376	0.9376	**Spatial Filling**	0.9199	0.9199	**Prominence**	0.7381	0.7381
Kurtosis	0.6465	0.6795	**LHP**	0.6482	0.6505	**LHP**	0.4320	0.4843
LHP	0.5966	0.6616	**Teager Energy**	0.8277	0.8509	**STD**$_{acc'}$	0.6925	0.7054
Spatial Filling	0.6948	0.9348	AUC$_{C-curve}$	0.8668	0.8822	Simplicity	0.4314	0.4957
STD$_{xz}$	0.9225	0.9339	Entropy	0.8616	0.9078	Kurtosis	0.3904	0.6537
Entropy	0.7851	0.9299	Prominence	0.6919	0.8448	Spatial Filling	0.3694	0.5803
Skewness	0.6557	0.6624	Kurtosis	0.6117	0.6710	Entropy	0.5543	0.5857
P$_{4Peaks}$	0.6808	0.9303	P$_{4Peaks}$	0.6117	0.8642	Skewness	0.4025	0.5724
STD	0.5842	0.9361	Skewness	0.5446	0.662	STD$_{yz}$	0.3409	0.4561
Simplicity	0.5000	0.6577	Simplicity	0.5389	0.5522	STD	0.2307	0.4472
Teager Energy	0.4958	0.9029	STD$_{yz}$	0.5843	0.8191	STD$_{xz}$	0.1513	0.4400
STD$_{acc'}$	0.4402	0.9004	STD$_{acc'}$	0.4986	0.8531	P$_{4Peaks}$	0.0728	0.4247
Prominence	0.3963	0.5787	STD	0.4523	0.8381	AUC$_{C-curve}$	0.0166	0.4996
AUC$_{C-curve}$	0.3981	0.9081	STD$_{xz}$	-0.2667	0.1659	Teager Energy	-0.1354	0.2920

5.2.2.2 Multiclass Classifier

The second algorithm developed consists of using a sole multiclass classifier for the problem at hand. Seen that the cascade classifier naturally leads to an error accumulation there was interest in understanding how this limitation can be surpassed

and if this source of error can be diminished. Once again the algorithm was trained and tested in both datasets available using a LOO validation for the results. Since the feature selection score used for each classifier of the cascade approach is built for selection of features in a binary classification problem, a different path was undertaken with feature selection being performed by a wrapper approach. This means all possible feature combinations were tested and a metric of performance was used to select the best combination. The limitation of this approach is that it demands a higher amount of computational power to select the features for the final classifiers used, so in order to diminish this effect combinations which contained features that presented a correlation of over 90% were excluded from the start. A flow diagram of the feature selection process can be seen in Figure 5.14 with one iteration of the LOO validation in this approach depicted in Figure 5.15.

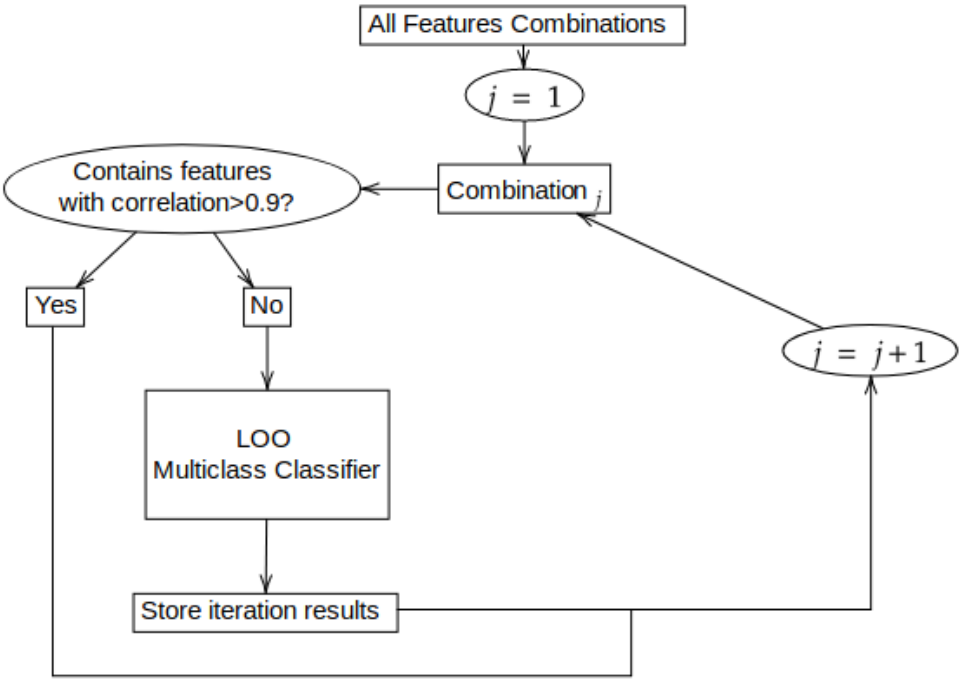

Figure 5.14: Wrapper Approach for feature selection

The results obtained for each combination are the general accuracy and sensitivities and specificities for each class calculated as described in 5.27, 5.28 and 5.29. In order to decide which combination of features presented the best results, the average geometric mean(GM) was used. This metric has the advantage of relating the sensitivity and specificity, allowing to choose a classifier which presents the best balance between these two metrics. It was initially calculated for each class of each subject and then averaged in the subjects, and again averaged among classes to present the

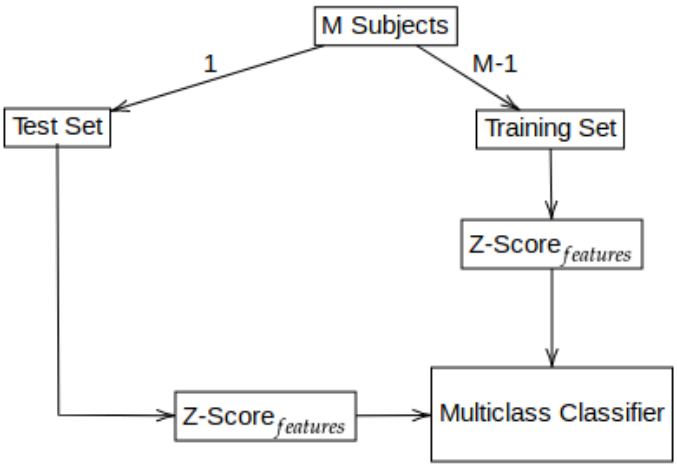

Figure 5.15: One iteration of the LOO algorithm using the sole multiclass classifier

final metric of the classifier. The combination chosen was the one which measured the maximum final GM. For each class the calculation is performed as follows:

$$GM_{class} = \sqrt{Sensitivity_{class} Specificity_{class}} \tag{5.25}$$

5.3 Results

5.3.1 Cascading Classifier

A summary of the features chosen for each classifier can be found in Table 5.4. To perform LOO validation, one subject composed the test set whilst the remaining composed the training set. This process was repeated iteratively until all subjects had been part of the test set. An iteration of the LOO validation is depicted in Figure 5.16. During training features for each classifier were normalised with the Z-Score formula as in 5.26 with f_i representing the raw value of a feature, μ_i the mean of the same feature in all the windows selected and σ_i the standard deviation. The mean and standard deviation of each normalisation were posteriorly used for the correspondent z-scoring in the test data.

$$z_i = \frac{f_i - \mu_i}{\sigma_i} \tag{5.26}$$

Table 5.4: Features selected by a FSS for each internal classifier of the cascade approach

	Classifier 1	**Classifier 2**	**Classifier 3**
Protocol - Top ACC	STD_{xz}	Simplicity Teager Energy	-
Protocol - Bottom ACC	STD	Prominence STD_{xz}	-
Real-Life Data	STD_y_z Kurtosis	Spatial Filling LHP Teager Energy	Prominence LHP $STD_{acc'}$

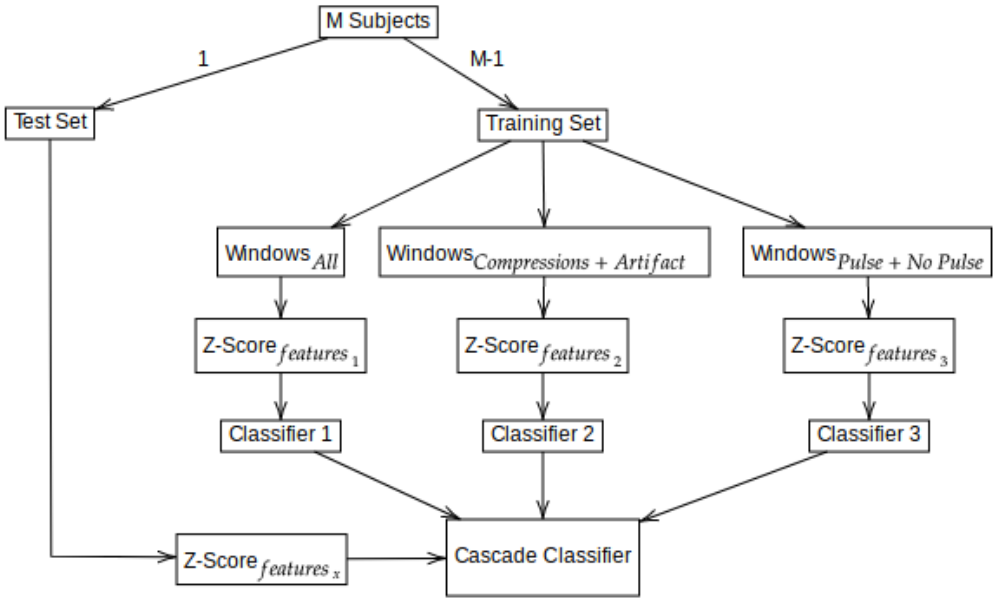

Figure 5.16: One iteration of the LOO validation, when using the cascade classifier approach

From this approach several measures of performance were extracted, specifically:

- Using the confusion matrix(size 3x3 for protocol data, and 4x4 for real life data) obtained when comparing the final labels provided by the whole cascade classifier with the ground truth labels, it is possible to extract the general accuracy of the algorithm($Accu_{final}$), and a general sensitivity and specificity for each class. Before doing so however, it is necessary to multiply the matrix by the inverse of the real probability of a window of each class appearing, in order to diminish the error brought forward by the class imbalance present in the data. By doing so, the confusion matrix becomes virtually balanced providing a unskewed analysis of the behaviour of the solutions developed. An example of a possible confusion matrix, is depicted in Figure 5.17, with true

positives(TP), false positives(FP), true negatives(TN) and false negatives(FN) showed for class 1. General accuracy, sensitivity for each class and specificity for each class were then calculated as follows in 5.27, 5.28 and 5.29 respectively:

$$Accu_{final} = \frac{\sum_{class=1}^{n_{class}} TP_{class}}{\sum_{class=1}^{n_{class}} (TP_{class} + FN_{class})} \tag{5.27}$$

$$Sensitivity_{class} = \frac{TP_{class}}{TP_{class} + FN_{class}} \tag{5.28}$$

$$Specificity_{class} = \frac{TN_{class}}{TN_{class} + FP_{class}} \tag{5.29}$$

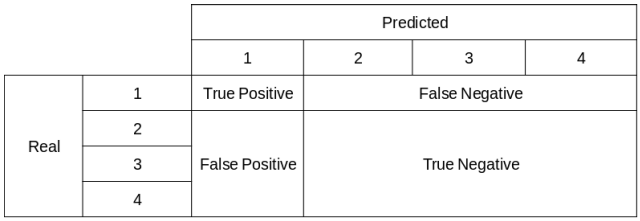

Figure 5.17: Example of a confusion matrix

- Accuracy, Sensitivity and Specificity for each individual classifier used inside the cascade classifier logic. These calculations were performed so that individual analysis of the performance of each step was possible, with the effect of errors from previous steps unaccounted. Since each of the classifiers represents a binary classification problem, calculations are made with the commonly used formulas

$$Accuracy = \frac{TP + TN}{TP + FN + TN + FP} \tag{5.30}$$

$$Sensitivity = \frac{TP}{TP + FN} \tag{5.31}$$

$$Specificity = \frac{TN}{TN + FP} \tag{5.32}$$

The results obtained on the acquired data can be found in Tables 5.5 and 5.7, whilst the results pertaining the real life data set are depicted in Tables 5.6 and 5.8. Observation of the results in the time domain allows to perform a better analysis of

the limitations of the algorithm with an example of a full signal classification visible in Figure 5.18.

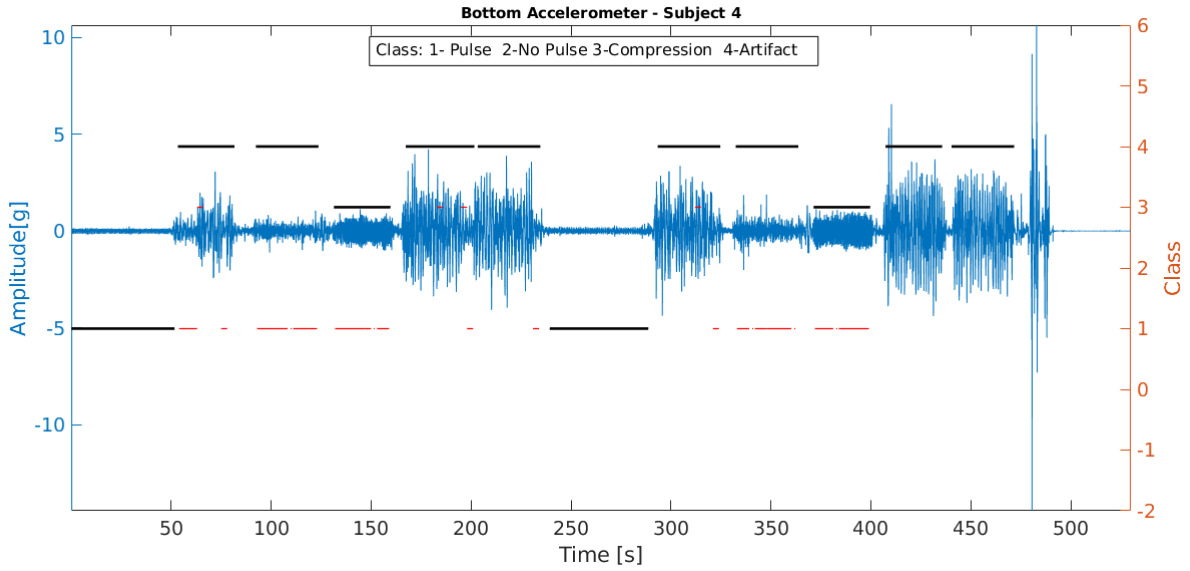

Figure 5.18: Protocol Data: Subject 4 - Full Signal Output of the cascade classifier. Black line represents the ground truth label and red the predicted output

Table 5.5: Results for the internal classifiers of the algorithm - Protocol Data

Patient #		Classifier 1 Pulse vs (Compression & Artifact)			Classifier 2 Compression vs Artifact		
		Accu.	Sens.	Spec.	Accu.	Sens.	Spec.
1	Top	0.9604	1.0000	0.9208	0.7600	1.0000	0.5200
	Bottom	1.0000	1.0000	1.0000	0.9430	1.0000	0.8861
2	Top	0.9740	1.0000	0.9479	0.6500	0.3000	1.0000
	Bottom	1.0000	1.0000	1.0000	0.9472	0.9500	0.9444
3	Top	0.8925	1.0000	0.7849	0.9269	0.8889	0.9469
	Bottom	1.0000	1.0000	1.0000	0.9527	1.0000	0.9054
4	Top	0.8700	1.0000	0.7400	0.9146	1.0000	0.8293
	Bottom	0.9588	1.0000	0.9175	0.9494	1.0000	0.8987
5	Top	0.8608	1.0000	0.7216	0.8685	0.7857	0.9512
	Bottom	0.9255	1.0000	0.8511	0.9196	0.9444	0.8947
6	Top	0.9612	1.0000	0.9223	0.8418	0.7778	0.9059
	Bottom	0.9802	1.0000	0.9604	0.9940	1.0000	0.9880
7	Top	0.9895	1.0000	0.9789	0.8056	0.6111	1.0000
	Bottom	0.9844	1.0000	0.9688	0.9252	0.8889	0.9615
8	Top	0.8150	0.9667	0.6633	0.9097	0.9444	0.8750
	Bottom	0.9309	1.0000	0.8617	0.8527	0.8000	0.9054
9	Top	0.9375	1.0000	0.8750	0.8590	1.0000	0.7179
	Bottom	0.9947	1.0000	0.9895	0.8990	0.8889	0.9091
10	Top	0.8687	1.0000	0.7374	0.8810	1.0000	0.7619
	Bottom	0.9625	0.9667	0.9583	0.9250	1.0000	0.8500
11	Top	0.9947	1.0000	0.9894	0.5227	0.0417	1.0000
	Bottom	1.0000	1.0000	1.0000	0.9075	0.8421	0.9730
12	Top	0.9348	1.0000	0.8696	0.8919	1.0000	0.7838
	Bottom	1.0000	1.0000	1.0000	0.8896	0.8333	0.9459
Mean±std	Top	0.92 ± 0.06	0.99 ± 0.01	0.85 ± 0.11	0.81 ± 0.12	0.78 ± 0.31	0.84 ± 0.16
	Bottom	0.98 ± 0.03	0.99 ± 0.01	0.96 ± 0.05	0.93 ± 0.04	0.93 ± 0.08	0.92 ± 0.04

Table 5.6: Results for the internal classifiers of the algorithm - Real Data

Patient #	Classifier 1 (Pulse & No Pulse) vs (CPR & Artifact)			Classifier 2 Compression vs Artifact			Classifier 3 Pulse vs No Pulse		
	Accu.	Sens.	Spec.	Accu.	Sens.	Spec.	Accu.	Sens.	Spec.
1	0.8932	0.9735	0.8129	0.7602	0.8815	0.6389	0.4788	0.2131	0.7444
2	0.7408	0.9940	0.4877	0.6534	0.7317	0.5750	0.5374	0.6070	0.4677
3	0.9520	0.9896	0.9144	0.9440	0.9880	0.9000	0.5641	0.4919	0.6364
4	0.7533	1.0000	0.5067	0.9146	1.0000	0.8293	0.6195	0.7152	0.5238
5	0.8813	0.9822	0.7804	0.8241	0.9944	0.6538	0.5237	0.1000	0.9474
Mean ± std	0.84 ± 0.09	0.99 ± 0.01	0.70 ± 0.19	0.82 ± 0.12	0.92 ± 0.12	0.72 ± 0.14	0.54 ± 0.05	0.43 ± 0.26	0.66 ± 0.19

Table 5.7: Final Results of the cascade classifier - Protocol Data

Patient #		Accu Final	Pulse		Compression		Artifact	
			Sens.	Spec.	Sens.	Spec.	Sens.	Spec.
1	Top	0.6667	1.0000	0.8267	1.0000	0.6733	0	1.0000
	Bottom	0.6892	1.0000	0.5288	0.2222	0.9494	0.7342	1.0000
2	Top	0.4088	1.0000	0.4618	0.2000	0.6645	0.0526	1.0000
	Bottom	0.5648	1.0000	0.4306	0	0.9514	0.7639	1.0000
3	Top	0.6574	1.0000	0.7230	0.9722	0.7632	0	1.0000
	Bottom	0.8604	1.0000	0.8311	1.0000	0.9324	0.5270	1.0000
4	Top	0.4074	1.0000	0.3245	0.2222	0.7866	0	1.0000
	Bottom	0.5359	1.0000	0.3291	0	0.9684	0.5949	1.0000
5	Top	0.6667	1.0000	0.5000	1.0000	1.0000	0	1.0000
	Bottom	0.7081	1.0000	0.5819	0.5556	0.9605	0.4737	0.9722
6	Top	0.4630	1.0000	0.4212	0.2778	0.7176	0	1.0000
	Bottom	0.7965	1.0000	0.6948	0.6667	1.0000	0.7229	1.0000
7	Top	0.7205	1.0000	0.8777	0.8333	0.6883	0.2987	1.0000
	Bottom	0.8917	1.0000	0.8846	0.7222	0.9936	0.9231	0.9444
8	Top	0.6667	1.0000	0.7437	1.0000	0.7563	0	1.0000
	Bottom	0.7743	1.0000	0.8176	0.8500	0.9324	0.5000	0.9250
9	Top	0.6667	1.0000	0.8269	1.0000	0.6731	0	1.0000
	Bottom	0.8764	1.0000	0.8701	0.8889	1.0000	0.7403	0.9444
10	Top	0.6000	1.0000	0.7071	0.8667	0.7262	0	1.0000
	Bottom	0.5708	1.0000	0.4563	0.1875	0.8875	0.5000	1.0000
11	Top	0.6515	1.0000	0.8314	0.9545	0.6458	0	1.0000
	Bottom	0.8487	1.0000	0.7137	0.6316	1.0000	0.7432	0.9737
12	Top	0.6667	1.0000	0.7770	1.0000	0.7230	0	1.0000
	Bottom	0.8729	1.0000	0.8784	0.8889	0.9797	0.7162	0.9444
Mean±std	Top	0.60 ± 0.11	1.00 ± 0.00	0.67 ± 0.19	0.78 ± 0.33	0.73 ± 0.09	0.03 ± 0.09	1.00 ± 0.00
	Bottom	0.75 ± 0.13	1.00 ± 0.00	0.67 ± 0.20	0.55 ± 0.36	0.96 ± 0.03	0.66 ± 0.14	0.97 ± 0.03

Table 5.8: Final Results of the cascade Classifier - Real Data

Patient #	Accu_{final}	Pulse		No Pulse		Compression		Artifact	
		Sens.	Spec.	Sens.	Spec.	Sens.	Spec.	Sens.	Spec.
1	0.4736	0.6393	0.5944	0.2667	0.7502	0.9778	0.9574	0.0000	0.9926
2	0.4501	0.9639	0.4683	0.0323	0.9605	0.7439	0.8179	0.0000	1.0000
3	0.5277	0.8844	0.6359	0.1818	0.8633	0.9940	0.8543	0.0000	1.0000
4	0.5435	0.9358	0.5993	0.2857	0.8404	1.0000	0.9675	0.0000	1.0000
5	0.5481	0.5533	0.7584	0.5789	0.7656	1.0000	0.8534	0.0000	1.0000
Mean±std	0.51 ± 0.04	0.80 ± 0.19	0.61 ± 0.10	0.27 ± 0.20	0.84 ± 0.08	0.94 ± 0.11	0.89 ± 0.07	0.00 ± 0.00	1.00 ± 0.00

5.3.2 Multiclass Classifier

Using the feature selection wrapper approach described previously, it was possible to select the combinations which provided the maximum GM. The features chosen for each sensor tested are summarised in Table 5.9. Using these combinations general accuracy, sensitivities and specificities of each classifier were also calculated with the results depicted in Tables 5.10 and 5.11. A time domain output of the classifier is displayed in Figure 5.19.

Table 5.9: Features selected for the multiclass classifer of each sensor

	Features
Protocol Data - Top ACC	STD , PM, STD_{xz}, SF, SIM
Protocol Data - Bottom ACC	PM , LHP , STD_{xz} , STD_{yz} , KU , SK , $STD_{acc'}$, EN , SIM
Real Life Data	TE , Prominence , STD_{yz} , $STD_{acc'}$, SF

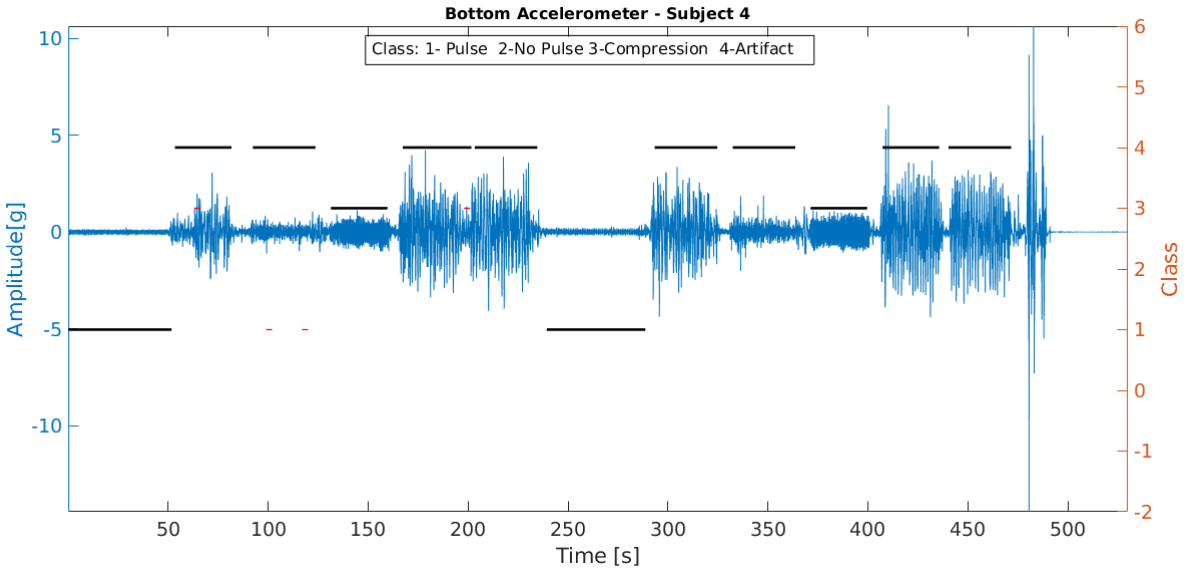

Figure 5.19: Protocol Data: Subject 4 - Full Bottom ACC Signal Output of the multiclass classifier. Black line represents the ground truth label and red the predicted output

Table 5.10: Final results of the multiclass approach - Protocol Data

Patient #		$Accu_{final}$	Pulse		Compression		Artifact	
			Sens.	Spec.	Sens.	Spec.	Sens.	Spec.
1	Top	0.9600	1.0000	0.9867	1.0000	0.9533	0.8800	1.0000
	Bottom	0.9916	1.0000	1.0000	1.0000	0.9873	0.9747	1.0000
2	Top	0.8702	1.0000	0.9803	0.6500	1.0000	0.9605	0.8250
	Bottom	0.9907	1.0000	1.0000	1.0000	0.9861	0.9722	1.0000
3	Top	0.9264	1.0000	0.9386	0.9722	0.9649	0.8070	0.9861
	Bottom	0.9595	1.0000	1.0000	1.0000	0.9392	0.8784	1.0000
4	Top	0.8780	1.0000	0.9695	1.0000	0.8476	0.6341	1.0000
	Bottom	0.9705	1.0000	0.9873	1.0000	0.9684	0.9114	1.0000
5	Top	0.8397	1.0000	0.9268	0.7143	0.9756	0.8049	0.8571
	Bottom	0.9561	1.0000	0.9737	1.0000	0.9605	0.8684	1.0000
6	Top	0.9473	1.0000	0.9824	0.8889	0.9941	0.9259	0.9444
	Bottom	0.9880	1.0000	0.9819	1.0000	1.0000	0.9639	1.0000
7	Top	0.9259	1.0000	1.0000	0.7778	1.0000	1.0000	0.8889
	Bottom	0.9757	0.9655	0.9808	1.0000	1.0000	0.9615	0.9828
8	Top	0.8889	0.8667	0.9750	1.0000	0.9250	0.8000	0.9333
	Bottom	0.9124	0.9412	0.9730	0.8500	0.9853	0.9459	0.9103
9	Top	0.8958	0.9310	0.9936	1.0000	0.8846	0.7564	0.9655
	Bottom	0.9913	1.0000	1.0000	1.0000	0.9870	0.9740	1.0000
10	Top	0.8452	1.0000	0.9107	1.0000	0.8571	0.5357	1.0000
	Bottom	0.9389	0.9667	0.9938	0.8750	0.9938	0.9750	0.9208
11	Top	0.7570	0.9667	0.9931	0.3182	1.0000	0.9861	0.6424
	Bottom	0.9717	0.9667	1.0000	0.8750	0.9938	0.9750	0.9208
12	Top	0.9324	1.0000	1.0000	1.0000	0.8986	0.7973	1.0000
	Bottom	0.9955	1.0000	1.0000	1.0000	0.9932	0.9865	1.0000
Mean±std	Top	0.89 ± 0.06	0.98 ± 0.04	0.97 ± 0.03	0.86 ± 0.21	0.94 ± 0.06	0.82 ± 0.14	0.92 ± 0.11
	Bottom	0.97 ± 0.03	0.99 ± 0.02	0.99 ± 0.01	0.97 ± 0.05	0.98 ± 0.02	0.95 ± 0.04	0.98 ± 0.03

Table 5.11: Final results of the multiclass approach - Real Data

Patient #	$Accu_{final}$	Pulse		No Pulse		Compression		Artifact	
		Sens.	Spec.	Sens.	Spec.	Sens.	Spec.	Sens.	Spec.
1	0.5526	0.1639	0.9222	0.4111	0.7268	0.7185	0.9870	0.9167	0.7674
2	0.4790	0.2577	0.7289	0.2419	0.8899	0.8415	0.9333	0.5750	0.7533
3	0.5832	0.2554	0.9207	0.5455	0.6220	0.9820	0.9991	0.5500	0.9024
4	0.6829	0.6274	0.8568	0.5238	0.8161	0.9706	0.9837	0.6098	0.9206
5	0.5619	0.12	0.9444	0.5789	0.7056	0.8305	0.9744	0.7179	0.7918
Mean±std	0.57 ± 0.07	0.28 ± 0.20	0.87 ± 0.09	0.46 ± 0.14	0.75 ± 0.10	0.87 ± 0.11	0.98 ± 0.03	0.67 ± 0.15	0.83 ± 0.08

5.4 Discussion

5.4.1 Feature Engineering

An extensive feature engineering process was done in this work, with some different features than those used in previous works being extracted and tested. By observation of the tables referring to the feature selection process (5.1, 5.2 and 5.3) it is possible to observe that different features have different behaviour depending on the binary classification problem to which they are applied and also on the sensor being used. Success was achieved in obtaining features with high AUC for almost all the problems at hand. Nevertheless, redundancy was found between some features and for the binary problem of *Pulse/No Pulse* feature engineering proved partic-

ularly demanding. For one, there was a lack of *No Pulse* data available, which is understandable, when considering the challenges in performing real-life acquisitions. However, this lack of data makes it difficult to adequately study the characteristics of the signal when this state is present. It is also necessary to have in consideration that the lack of medical expertise for the annotation of the data might also be affecting the results. Despite pulse presence or its absence being defined by the arterial blood pressure, not always was there a secondary signal which measured this value and also due to the intensity of the scenario at hand, contamination of the data might have influenced the interpretation of the existent signals. In Figure 5.20 an ambiguous case is depicted with both sides, i.e., signal pre-compressions and post-compressions being labeled as pulse, despite the fact the pre-compression signal is considerably lower in amplitude.

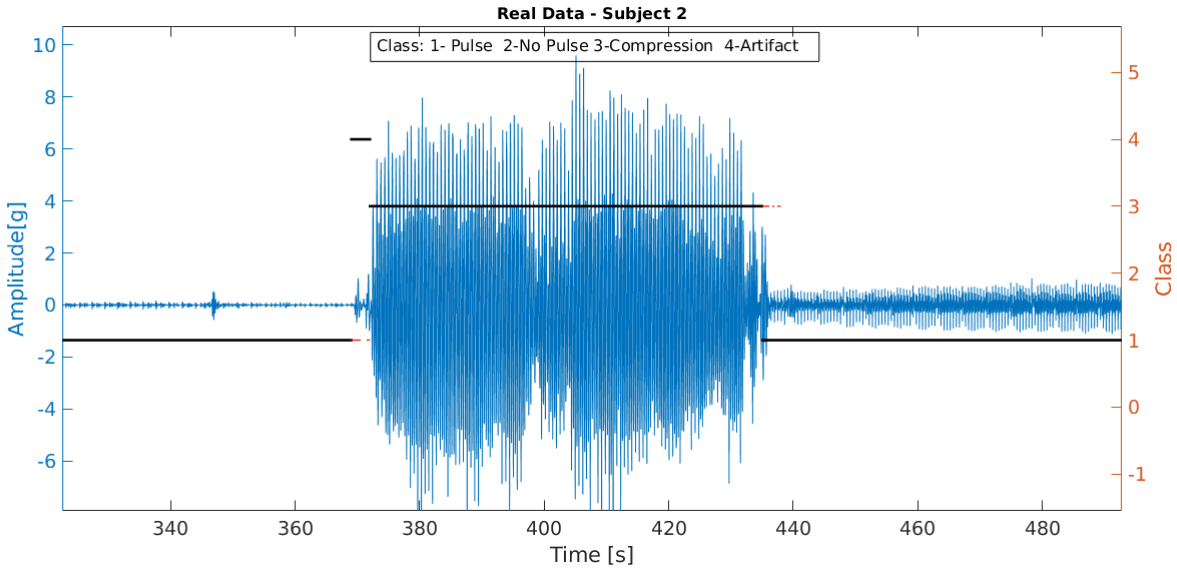

Figure 5.20: Real Data: Subject 2 - Segment Output of the cascade classifier. Black line represents the ground truth label and red the predicted output. Pulse segment, followed by compressions and afterwards pulse signal

Nevertheless, interesting developments are brought forward by the feature extraction performed in this work. For the first time in a accelerometer pulse detection problem, PSR features were extracted. This non-linear signal processing technique proved to be important with its features presenting very good AUC for different classification problems and were included in the final solutions developed for some of the sensors. Further study of the technique and extraction of features from the phase space might yet allow for further advances.

5.4.2 Classification

Firstly, regarding the protocol data acquired and its classification differents points can be discussed. By observation of Table 5.5 it is immediately visible that the bottom accelerometer presents better and more stable results as compared to the top accelerometer. This corroborates the conclusions of the previous chapter where this sensor was found to present a higher signal quality. Naturally, a higher quality signal allows for a more stable feature extraction. This effect is also visible, in Table 5.7 which shows the final results of the cascade classifier algorithm and in Table 5.10, relative to the multiclass classifier results. Although good results are in general present in the internal classifiers, when applying the full cascade classifier algorithm, there is a natural accumulation of error which diminish the performance considerably. Features selected for the first step of the algorithm in both sensors of this dataset are features of activity, so if a window corresponding to a lower activity artifact or compression than those present in the signals used for training is misclassified in this first step it will never present a correct result in the end, affecting both the pulse specificity and the sensitivity of the class to which it belongs. However, this effect is almost completely diminished when the multiclass classifier approach is used, which comes to prove that using a sole classifier might allow for a better characterisation of the classes present in the dataset than working with assumptions of activity and periodicity that might not always be linear. In Figure 5.21 it is possible to observe the misclassification of lower activity artifact windows.

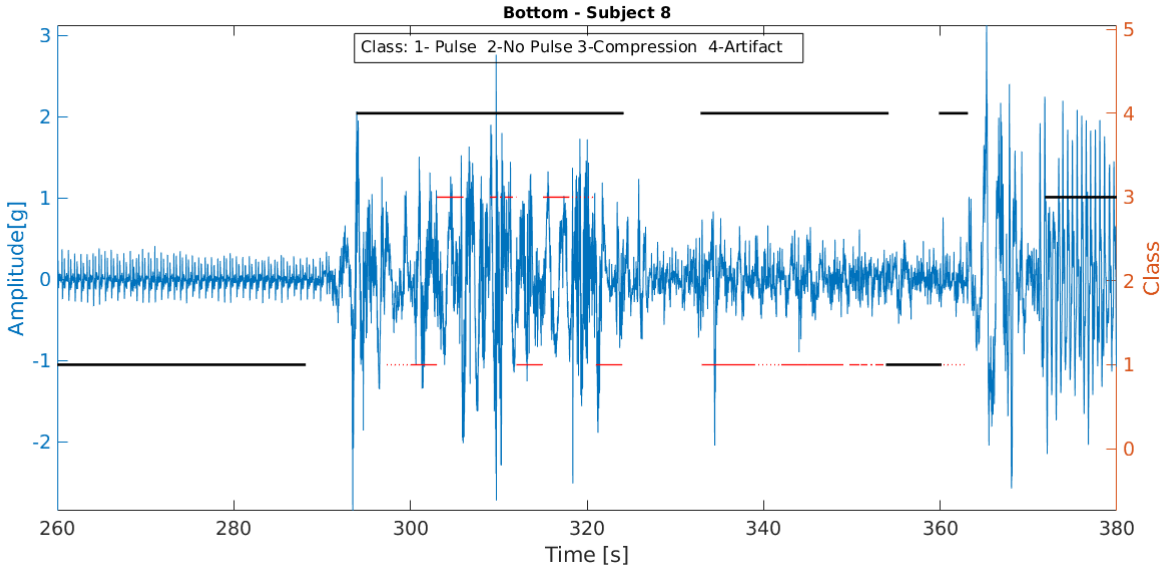

Figure 5.21: Protocol Data: Subject 8 - Segment Output of the cascade classifier. Black line represents the ground truth label and red the predicted output

Table 5.12: Results achieved by Dellimore *et al.*[1] using the real-life data

Patient #	Activity classification		Compression Periodicity classification		Pulse periodicity classification	
	Sens.	Spec.	Sens.	Spec.	Sens.	Spec.
1	1.0000	0.8390	0.7210	0.9140	0.3680	0.8330
2	1.0000	0.8333	0.9380	0.7880	0.7000	0.4000
3	0.9770	0.9180	0.9650	0.8940	1.0000	0.2350
4	1.0000	0.8690	1.0000	0.8240	0.2590	0.8000
5	0.9960	0.9220	0.9930	0.8460	0.7310	0.6580

The results achieved when training and testing with the real-life dataset are not as optimistic. In Table 5.6, which refers to the results of the internal classifiers of the first algorithm, it is observed that relatively good sensitivities and specificities are present in both the first and the second classifier. Conversely, poor results are achieved in the classification of *Pulse* and *No Pulse* windows. The results achieved in the previous work by Dellimore *et al.*, presented in the Table 5.12, present higher sensitivities and specificities in all the classifiers. However, it is necessary to take in consideration that in the previous work subject-dependent optimal thresholds were used, instead of automatic classification by a trained classifier which undoubtedly influences the results positively. This practice is not applicable in a real-life situation as prior knowledge of each subject undergoing CPR is non existent. It is also worth noting that, while performing data annotation some of the prior labels were altered which also influences the results. Most of these alterations were related to low activity artifacts, which were unidentified, leading to the existence of high activity and low activity artifact labels in the dataset. By training with both of these present in the signal it is possible to see in Table 5.8, which refers to the final results of the cascade classifier, that the sensitivity for artifact detection is zero. If it has a high activity it is labeled as *Compression* and if it presents a low activity it is immediately misclassified in the first step of the algorithm(depicted in Figures 5.22 and 5.23). It's worth mentioning though that *Compression* classification presents both high sensitity and specificity, whilst *Pulse* classification shows a high sensitivity and low specificity.

When testing with the second algorithm, i.e., the multiclass classifier, *Artifact* sensitivities are drastically increased, whilst also presenting high specificity. However, this increase leads to a drastic decrease in pulse sensitivity. *Pulse* and *No Pulse* classification still present limitations, which are to be expected as lack of absence of pulse data and data imbalance made it difficult to adequately study the problem. *Compression* classification maintains high sensitivity and specificity.

It's also important to remember that tests in the protocol data were performed on

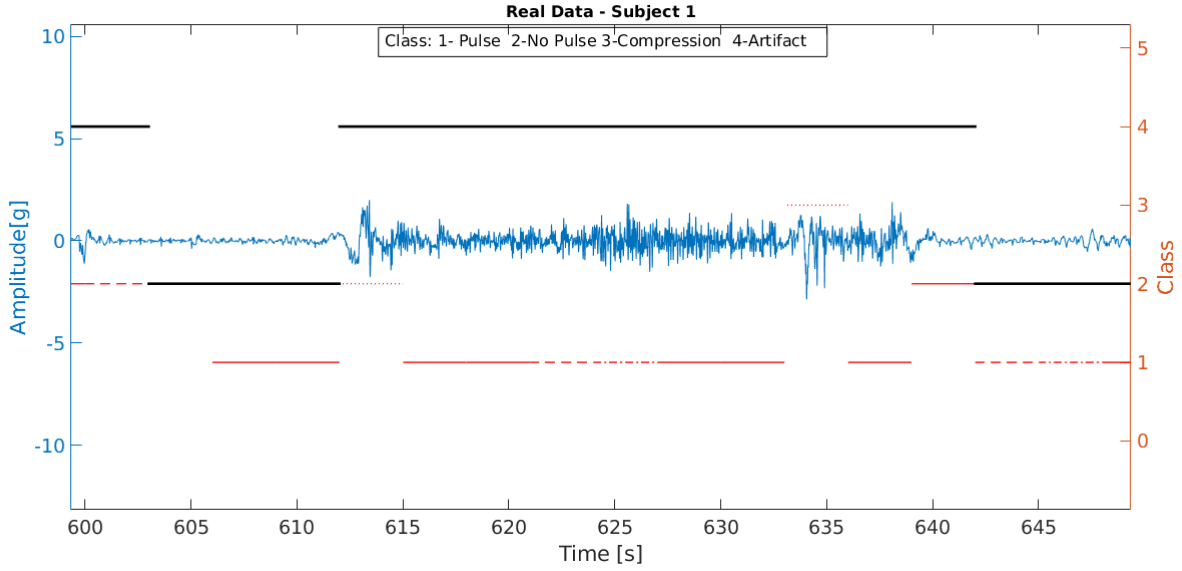

Figure 5.22: Real Data: Subject 1 - Segment Output of the cascade classifier. Black line represents the ground truth label and red the predicted output. Low activity artifact misclassified

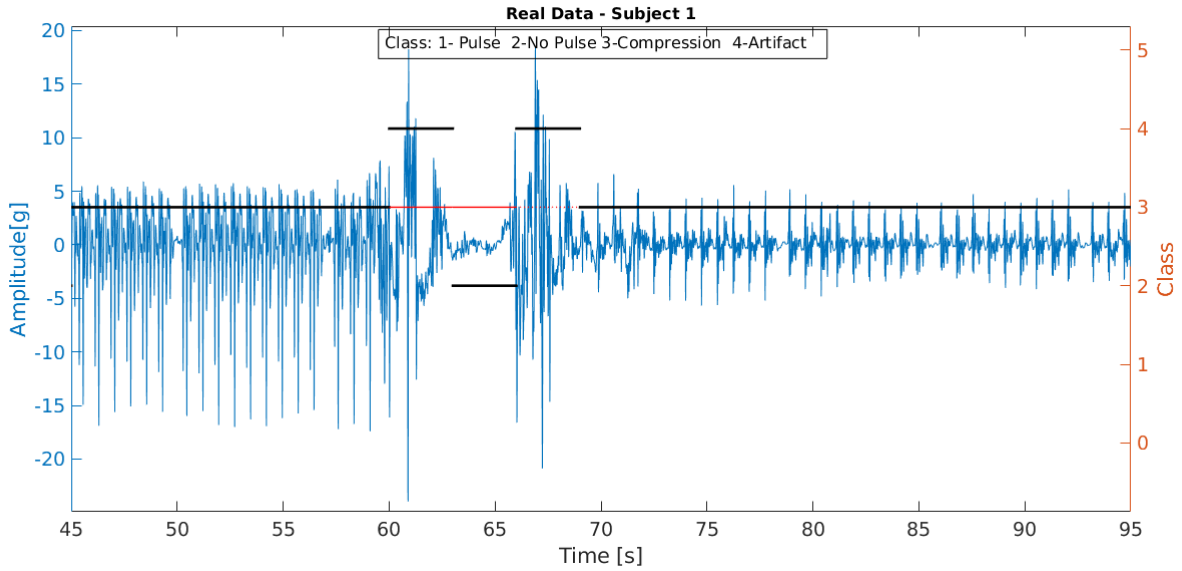

Figure 5.23: Real Data: Subject 1 - Segment Output of the cascade classifier. Black line represents the ground truth label and red the predicted output. High activity artifact misclassified

"clean" windows, i.e., transitions were marked during annotation and were removed from training and testing. This was not done in the real-life dataset annotation. Certainly, the very good results obtained in the acquired data are also influenced by this aspect and the results on the real-life dataset suffer, as data contamination by noise is present.

5.5 Conclusion and Future Work

Automatic pulse detection is no easy task, even more so when trying to do it in a cardiopulmonary resuscitation scenario. As discussed in the previous chapter a protocol was designed and data acquisition of 12 healthy volunteers took place in order to create a database, which along with a real-life data set composed of 5 patients undergoing CPR, was used to develop technical solutions.

Regarding the extensive feature engineering performed, success was achieved in finding new features which accurately characterise the domain space for several of the existent classification problems. The most interesting contribution arises from the extraction of features from the PSR of the signal.

In this chapter two approaches were developed not only for *Pulse/No Pulse* classification but also for classification of other common classes present in such a scenario, specifically *Compressions* and *Artifacts*. The first approach consisted of a cascade classifier, with two or three internal classifiers(depending of the dataset used). This approach proved not to be the best, due to the error accumulation that is intrinsic to it. To diminish this effect a sole multiclass classifier was also trained and tested, and it succeeded in improving some results in all datasets, with its effect in the protocol data being tremendous leading to exceptional results. This leads to the conclusion that it might be the best approach to develop future studies in this area.

The major conclusion derived from the simulated data is that sensor positioning is vital for signal quality and consequently to the results obtained with the data. Hence, further studies on the positioning of the sensor should be performed in order to estabilish a relative optimal position. This would allow for more consistent data which would allow for a more correct analysis of the properties of the signal.

Pulse presence and absence detection in the real-life signals did not show particularly good results. However, this was to be expected as data imbalance and the lack of *No Pulse* data available are main limitations in the dataset used. Nevertheless, low activity segments of the signal are easy to identify as shown by results of the internal classifiers of the first approach, and further signal processing techniques on these segments, such as running a pulse peak algorithm might provide interesting results. A multiclass classifier might also provide classification potential in this problem. Additionally, further studies in blood pressure assessment using ACC signals from the carotid also constitute an important step, as this is the vital sign which determines presence or absence of pulse.

It's important to take in consideration that the size of both datasets was limited and so no conclusions are definitive with further testing in an expanded dataset being necessary.

6

Conclusions

The aim of this thesis was to explore the use of accelerometers positioned in the neck area along the carotid for the development of pulse detection algorithms during cardiopulmonary resuscitation. Motivation for this study arises from the fact that current pulse assessment methods during resuscitation events are still prone to error, take too long and do not provide an objective measure of pulse. Hence, there is a need for a pulse detection technique which improves on the current State-of-the-Art techniques. Focus was also put on classifying different classes which are present during these interventions, namely compressions and artifacts. Being able to identify the different conditions would allow for a more optimal resuscitation process and improve low survival outcomes.

Since acquisition of accelerometer signals in real-life CPR scenarios in this thesis was not possible, a study with healthy volunteers was organised. The first challenge was to design a protocol for data acquisition which allowed for the simulation in controlled conditions of characteristics present in a real-life event. Using this protocol a dataset of 12 healthy volunteers was built. For each subject two accelerometer signals positioned along the carotid artery were measured synchronously with ECG and PPG. Although the work focused on the use of the accelerometer data, building a complete dataset is vital for allowing future research using the acquired data. Possible future work using the acquired dataset:

- Pulse Peak Detection: development of a algorithm for pulse rate extraction, evaluating the results using the heart rate extracted from the ECG. Compression Rate could also be extracted. This knowledge could be useful for providing feedback to rescuers allowing them to improve the care given.
- Pulse Wave Velocity: Feasibility of using two accelerometers positioned along the carotid for calculation of PWV
- Pulse Strength Assessment: Studying how pulse signal characteristic correlate

with PAT, with the ground truth values calculated from PPG and ECG signal;

Additionaly, a dataset of 5 patients undergoing CPR in a real-life scenario was available allowing comparison between the clinical data and the simulated data.

It was found that the developed protocol was able to accurately introduce periodic components simulating compression rate. Nevertheless, limitations were also found in the data with periodic artifacts being present instead of stochastic changes, which does not represent a realistic situation. It was possible to infer initially that sensor positioning at the neck plays an important role in the sensitivity of the measured signal content. In the acquisition of the simulated data two sensors were positioned in different positions in the neck area on the carotid artery, with one sensor being a higher position than the other. The bottom sensor demonstrated having a higher quality, with frequency components being more established in the signals measured. A more stable morphology throughout the different subjects was also evident. Future work on this would allow for higher quality signals, which in turn would allow for better study of signal's characteristics, as well as diminishing the morphology heterogeneity depending on sensor position.

Feature engineering based on domain knowledge and on fundamental information was performed in two different representations: the time domain and the phase space reconstruction of the signal. The latter presented a novel contribution on pulse detection applications and the features extracted in this representation showed potential in solving this detection problem.

Two approaches were implemented for the pulse detection classification and tested in both datasets. Regarding the use of a cascading classifier in the protocol data, it was found that despite relatively good performance being achieved in the individual steps of the method, the overall performance of this algorithm was relatively low for both sensor positions. Final accuracy averaged 60% and 75% for the top and bottom ACC respectively. The reason for this is that this approach suffers from intrinsic accumulation of error as a window misclassified in the first step will never be correctly classified in the end. Nevertheless, it was possible to observe that the bottom accelerometer signals presented better and less heterogeneous results which corroborates the previous insight on the signal quality of this sensor. When the second approach, i.e., the multiclass classifier was used on this data the effect was drastic with an average final accuracy of 89% in the top accelerometer data and 97% in the bottom accelerometer. Sensitivity and Specificity for each class in the bottom ACC all averaged $\geq 95\%$ with standard deviations $\leq 0.05\%$. However, it is important to note that transitions windows were excluded from training and testing

in this dataset, thus possibly improving the results.

Concerning the behaviour of a cascading classifier approach in the real life data it was found that due to the aforementioned source of error in this approach, all of the artifact windows were misclassified. This changes when using the multiclass classifier, with the average sensitivity of this class increasing to 67%. However, in this approach average artifact specificity decreased from 100% to 83%, which affected pulse sensitivity which becomes very low, averaging a value of 28%, whilst on the cascade classifier it averaged 89%. Nevertheless, this approach provided some interesting results and shows classification potential for the problem.

Pulse and *No Pulse* discrimination proved to be a difficult task with its performance in both approaches being fairly poor. However, it is important to note limitations faced: 1) there was a lack of data regarding absence of pulse ; 2) real-life signals are fairly contaminated with noise; 3) annotation was performed without medical expertise; 4) no windows were excluded from training and testing. Due to all of these no definitive conclusions can be taken from the results obtained.

Further work is necessary before a concrete viable solution is found as the limitations are various. Due to the limited datasets, it is difficult to study the problem thoroughly. Extension of the existing datasets is necessary, with the main requirement being the extraction of more data with absence of pulse. However, real-life data acquisition is difficult to arrange, hence suitable alternatives should be studied. Further work on simulated data and on the relation of pulse accelerometer signal with blood pressure(the physiological factor which determines presence or absence of pulse) could provide more insights on this problem.

In summary, despite several limitations imposed by the small datasets, the main goal of contributing with further knowledge for the innovation of the care given during CPR has been achieved.

Bibliography

[1] K. Dellimore, R. Wijshoff, C. Haarburger, V. Aarts, R. Derkx, J. van de Laar, K. Nammi, J. K. Russell, P. Hubner, F. Sterz, and J. Muehlsteff, "Towards an algorithm for automatic accelerometer-based pulse presence detection during cardiopulmonary resuscitation," in *2016 38th Annual International Conference of the IEEE Engineering in Medicine and Biology Society (EMBC)*, (Orlando, FL, USA), pp. 3531–3534, IEEE, Aug. 2016.

[2] S. Mader, *Understanding Human Anatomy and Physiology.* 5th ed., 2004.

[3] G. J. Tortora and B. Derrickson, *Principles of Anatomy and Physiology.* 12th ed., 2009.

[4] M. Elgendi, "On the Analysis of Fingertip Photoplethysmogram Signals," *Current Cardiology Reviews*, vol. 8, pp. 14–25, June 2012.

[5] J. Muehlsteff, P. Carvalho, J. Henriques, R. P. Paiva, and H. Reiter, "Cardiac status assessment with a multi-signal device for improved home-based congestive heart failure management," in *2011 Annual International Conference of the IEEE Engineering in Medicine and Biology Society*, (Boston, MA), pp. 876–879, IEEE, Aug. 2011.

[6] J.-T. Gräsner *et al.*, "EuReCa ONE 27 Nations, ONE Europe, ONE Registry," *Resuscitation*, vol. 105, pp. 188–195, Aug. 2016.

[7] E. J. Benjamin *et al.*, "Heart Disease and Stroke Statistics—2018 Update: A Report From the American Heart Association," p. 426, Mar. 2018.

[8] C. Atwood, M. S. Eisenberg, J. Herlitz, and T. D. Rea, "Incidence of EMS-treated out-of-hospital cardiac arrest in Europe," *Resuscitation*, vol. 67, pp. 75–80, Oct. 2005.

[9] T. D. Rea, R. T. Donohoe, M. Bloomingdale, and M. S. Eisenberg, "CPR with Chest Compression Alone or with Rescue Breathing," *The New England Journal of Medicine*, p. 11, 2010.

[10] I. Hasselqvist-Ax, G. Riva, J. Herlitz, M. Rosenqvist, J. Hollenberg, P. Nordberg, M. Ringh, M. Jonsson, C. Axelsson, J. Lindqvist, T. Karlsson, and L. Svensson, "Early Cardiopulmonary Resuscitation in Out-of-Hospital Cardiac Arrest," *New England Journal of Medicine*, vol. 372, pp. 2307–2315, June 2015.

[11] B. S. Abella, J. P. Alvarado, H. Myklebust, D. P. Edelson, A. Barry, N. O'Hearn, T. L. V. Hoek, and L. B. Becker, "Quality of Cardiopulmonary Resuscitation During In-Hospital Cardiac Arrest," p. 6, 2005.

[12] F. Adnet, M. N. Triba, S. W. Borron, F. Lapostolle, H. Hubert, P.-Y. Gueugniaud, J. Escutnaire, A. Guenin, A. Hoogvorst, C. Marbeuf-Gueye, P.-G. Reuter, N. Javaud, E. Vicaut, and S. Chevret, "Cardiopulmonary resuscitation duration and survival in out-of-hospital cardiac arrest patients," *Resuscitation*, vol. 111, pp. 74–81, Feb. 2017.

[13] J. Soar, J. P. Nolan, B. W. Böttiger, G. D. Perkins, C. Lott, P. Carli, T. Pellis, C. Sandroni, M. B. Skrifvars, G. B. Smith, K. Sunde, C. D. Deakin, R. W. Koster, K. G. Monsieurs, and N. I. Nikolaou, "European Resuscitation Council Guidelines for Resuscitation 2015," *Resuscitation*, vol. 95, pp. 100–147, Oct. 2015.

[14] S. Brearley, C. P. Shearman, and M. H. Simms, "Peripheral pulse palpation: An unreliable physical sign," *Annals of the Royal College of Surgeons of England*, vol. 74, pp. 169–171, 1992.

[15] M. Lundin, J.-P. Wiksten, T. Peräkylä, O. Lindfors, H. Savolainen, J. Skyttä, and M. Lepäntalo, "Distal Pulse Palpation: Is It Reliable?," *World Journal of Surgery*, vol. 23, pp. 252–255, Mar. 1999.

[16] C. A. Graham and N. F. Lewis, "Evaluation of a new method for the carotid pulse check in cardiopulmonary resuscitation," *Resuscitation*, vol. 53, pp. 37–40, Apr. 2002.

[17] B. Eberle, W. F. Dick, T. Schneider, G. Wisser, S. Doetsch, and I. Tzanova, "Checking the carotid pulse check: Diagnostic accuracy of first responders in patients with and without a pulse," vol. 33, pp. 107–116, 1996.

[18] J. Muehlsteff, K. Dellimore, V. Aarts, R. Derkx, C. Peiker, and C. Meyer, "Pulse detection with a single accelerometer placed at the carotid artery: Performance in a real-life diagnostic test during acute hypotension," in *2015 37th Annual International Conference of the IEEE Engineering in Medicine and Biology Society (EMBC)*, (Milan), pp. 434–437, IEEE, Aug. 2015.

[19] R. Couceiro, P. Carvalho, R. P. Paiva, J. Muehlsteff, J. Henriques, V. Schulze, A. Ritz, M. Kelm, and C. Meyer, "Characterization of surrogate parameters for blood pressure regulation in neurally-mediated syncope," in *2013 35th Annual International Conference of the IEEE Engineering in Medicine and Biology Society (EMBC)*, (Osaka), pp. 5381–5385, IEEE, July 2013.

[20] T. Rocha, S. a. Paredes, R. Cabiddu, R. Couceiro, P. Carvalho, and J. Henriques, "A tool for ECG analysis as a module of a tele-monitoring system," p. 2, 2015.

[21] R. P. Paiva, P. Carvalho, R. Couceiro, J. Henriques, M. Antunes, I. Quintal, and J. Muehlsteff, "Beat-to-beat systolic time-interval measurement from heart sounds and ECG," *Physiological Measurement*, vol. 33, pp. 177–194, Feb. 2012.

[22] R. Couceiro, P. Carvalho, R. P. Paiva, J. Muehlsteff, J. Henriques, C. Eickholt, C. Brinkmeyer, M. Kelm, and C. Meyer, "Real-Time Prediction of Neurally Mediated Syncope," *IEEE Journal of Biomedical and Health Informatics*, vol. 20, pp. 508–520, Mar. 2016.

[23] M. Alnaeb, N. Alobaid, A. Seifalian, D. Mikhailidis, and G. Hamilton, "Optical Techniques in the Assessment of Peripheral Arterial Disease," *Current Vascular Pharmacology*, vol. 5, pp. 53–59, Jan. 2007.

[24] H. K. Walker, W. D. Hall, and J. W. Hurst, *Clinical Methods: The History, Physical, and Laboratory Examinations*. Boston: Butterworths, 3rd ed., 1990.

[25] K. G. Lurie, E. C. Nemergut, D. Yannopoulos, and M. Sweeney, "The Physiology of Cardiopulmonary Resuscitation:," *Anesthesia & Analgesia*, vol. 122, pp. 767–783, Mar. 2016.

[26] J. P. Ornato and M. A. Peberdy, *Cardiopulmonary Resuscitation*. Totowa, N.J.: Humana Press, 2005. OCLC: 60948226.

[27] J. Muehlsteff, K. Dellimore, V. Aarts, C. Brinkmeyer, C. Eickholt, M. Kelm, and C. Meyer, "Feasibility of pulse presence and pulse strength assessment during head-up tilt table testing using an accelerometer located at the carotid

artery," in *2014 36th Annual International Conference of the IEEE Engineering in Medicine and Biology Society*, (Chicago, IL), pp. 894–897, IEEE, Aug. 2014.

[28] V. T. van Hees, L. Gorzelniak, E. C. Dean León, M. Eder, M. Pias, S. Taherian, U. Ekelund, F. Renström, P. W. Franks, A. Horsch, and S. Brage, "Separating Movement and Gravity Components in an Acceleration Signal and Implications for the Assessment of Human Daily Physical Activity," *PLoS ONE*, vol. 8, p. e61691, Apr. 2013.

[29] L. Giovangrandi, O. T. Inan, R. M. Wiard, M. Etemadi, and G. T. A. Kovacs, "Ballistocardiography — A method worth revisiting," in *2011 Annual International Conference of the IEEE Engineering in Medicine and Biology Society*, (Boston, MA), pp. 4279–4282, IEEE, Aug. 2011.

[30] B. Silva, J. Muehlsteff, R. Couceiro, J. Henriques, and P. Carvalho, "Artifact detection in accelerometer signals acquired from the carotid," in *2017 39th Annual International Conference of the IEEE Engineering in Medicine and Biology Society (EMBC)*, (Jeju Island, South Korea), pp. 135–138, IEEE, July 2017.

[31] V. Aarts, K. H. Dellimore, R. Wijshoff, R. Derkx, J. van de Laar, and J. Muehlsteff, "Performance of an accelerometer-based pulse presence detection approach compared to a reference sensor," in *2017 IEEE 14th International Conference on Wearable and Implantable Body Sensor Networks (BSN)*, (Eindhoven, Netherlands), pp. 165–168, IEEE, May 2017.

[32] R. Gravina, P. Alinia, H. Ghasemzadeh, and G. Fortino, "Multi-sensor fusion in body sensor networks: State-of-the-art and research challenges," *Information Fusion*, vol. 35, pp. 68–80, May 2017.

[33] W.-Y. Chung, S. Bhardwaj, A. Punvar, D.-S. Lee, and R. Myllylae, "A Fusion Health Monitoring Using ECG and Accelerometer sensors for Elderly Persons at Home," in *2007 29th Annual International Conference of the IEEE Engineering in Medicine and Biology Society*, (Lyon, France), pp. 3818–3821, IEEE, Aug. 2007.

[34] D. Curone, A. Tognetti, E. L. Secco, G. Anania, N. Carbonaro, D. De Rossi, and G. Magenes, "Heart Rate and Accelerometer Data Fusion for Activity Assessment of Rescuers During Emergency Interventions," *IEEE Transactions on Information Technology in Biomedicine*, vol. 14, pp. 702–710, May 2010.

[35] E. M. Tapia, S. S. Intille, W. Haskell, K. Larson, J. Wright, A. King, and R. Friedman, "Real-Time Recognition of Physical Activities and Their Intensities Using Wireless Accelerometers and a Heart Rate Monitor," in *2007 11th IEEE International Symposium on Wearable Computers*, (Boston, MA, USA), pp. 1–4, IEEE, Oct. 2007.

[36] J. Wang, R. Chen, X. Sun, M. F. She, and Y. Wu, "Recognizing Human Daily Activities From Accelerometer Signal," *Procedia Engineering*, vol. 15, pp. 1780–1786, 2011.

[37] D. H. Phan, S. Bonnet, R. Guillemaud, E. Castelli, and N. Y. Pham Thi, "Estimation of respiratory waveform and heart rate using an accelerometer," in *2008 30th Annual International Conference of the IEEE Engineering in Medicine and Biology Society*, (Vancouver, BC), pp. 4916–4919, IEEE, Aug. 2008.

[38] D. Morillo, J. Ojeda, L. Foix, and A. Jimenez, "An Accelerometer-Based Device for Sleep Apnea Screening," *IEEE Transactions on Information Technology in Biomedicine*, vol. 14, pp. 491–499, Mar. 2010.

[39] O. T. Inan, P.-F. Migeotte, K.-S. Park, M. Etemadi, K. Tavakolian, R. Casanella, J. Zanetti, J. Tank, I. Funtova, G. K. Prisk, and M. Di Rienzo, "Ballistocardiography and Seismocardiography: A Review of Recent Advances," *IEEE Journal of Biomedical and Health Informatics*, vol. 19, pp. 1414–1427, July 2015.

[40] L. Atallah, B. Lo, R. King, and G.-Z. Yang, "Sensor Positioning for Activity Recognition Using Wearable Accelerometers," *IEEE Transactions on Biomedical Circuits and Systems*, vol. 5, pp. 320–329, Aug. 2011.

[41] M. Jaeger, M. Mueller, D. Wettach, T. Oezkan, J. Motsch, T. Schauer, R. Jaeger, and A. Bolz, "First-aid sensor system: New methods for single-point detection and analysis of vital parameters such as pulse and respiration," in *2007 29th Annual International Conference of the IEEE Engineering in Medicine and Biology Society*, (Lyon, France), pp. 2928–2931, IEEE, Aug. 2007.

[42] R. W. Wijshoff, T. van der Sar, W. H. Peeters, R. Bezemer, P. Aelen, I. W. Paulussen, S. C. Ordelman, A. Venema, P. F. van Berkom, R. M. Aarts, P. H. Woerlee, G.-J. Scheffer, and G. J. Noordergraaf, "Detection of a spontaneous pulse in photoplethysmograms during automated cardiopulmonary resuscitation in a porcine model," *Resuscitation*, vol. 84, pp. 1625–1632, Nov. 2013.

[43] C. Sandroni and G. Ristagno, "End-tidal CO2 to detect recovery of spontaneous circulation during cardiopulmonary resuscitation: We are not ready yet," *Resuscitation*, vol. 104, pp. A5–A6, July 2016.

[44] C. T. Lui, K. M. Poon, and K. L. Tsui, "Abrupt rise of end tidal carbon dioxide level was a specific but non-sensitive marker of return of spontaneous circulation in patient with out-of-hospital cardiac arrest," *Resuscitation*, vol. 104, pp. 53–58, July 2016.

[45] B. Silva, J. Muehlsteff, R. Couceiro, J. Henriques, C. Peiker, C. Meyer, and P. Carvalho, "Robust carotid pulse detection using accelerometry and electrocardiography," in *2017 IEEE 3rd International Forum on Research and Technologies for Society and Industry (RTSI)*, (Modena, Italy), pp. 1–4, IEEE, Sept. 2017.

[46] T. Rocha, S. Paredes, P. de Carvalho, J. Henriques, and M. Antunes, "Phase space reconstruction approach for ventricular arrhythmias characterization," in *2008 30th Annual International Conference of the IEEE Engineering in Medicine and Biology Society*, (Vancouver, BC), pp. 5470–5473, IEEE, Aug. 2008.

[47] D. Kumar, "Automatic Heart Sound Analysis for Cardiovascular Disease," Sept. 2014.

[48] J. Frank, S. Mannor, and D. Precup, "Activity and Gait Recognition with Time-Delay Embeddings," p. 6, 2010.

[49] S. M. Krishnan, D. N. Dutt, Y. W. Chan, and V. Anantharaman, "Phase Space Analysis for Cardiovascular Signals," in *Advances in Cardiac Signal Processing* (U. R. Acharya, J. S. Suri, J. A. E. Spaan, and S. M. Krishnan, eds.), pp. 339–354, Berlin, Heidelberg: Springer Berlin Heidelberg, 2007.

[50] L. Cao, "Practical method for determining the minimum embedding dimension of a scalar time series," *Physica D: Nonlinear Phenomena*, vol. 110, pp. 43–50, Dec. 1997.

[51] R. Wang and K. Tang, "Feature Selection for Maximizing the Area Under the ROC Curve," in *2009 IEEE International Conference on Data Mining Workshops*, (Miami, FL, USA), pp. 400–405, IEEE, Dec. 2009.